Study on Optical Properties and Biocompatibility of Different Polymer-Gold
Nano-Composite Platforms for Opto-Micro Fluidic Applications

Michael Fanous

A Thesis

in

The Department

of

Mechanical and Industrial Engineering

Presented in Partial Fulfillment of the Requirements
for the Degree of Masters of Applied Science (Mechanical Engineering) at
Concordia University
Montreal, Quebec, Canada

February 2017

CONCORDIA UNIVERSITY
School of Graduate Studies

This is to certify that the thesis prepared

By: Michael Fanous

Entitled: Study on Optical Properties and Biocompatibility of Different Polymer-Gold
                   Nano-Composite Platforms for Opto-Micro Fluidic Applications

and submitted in partial fulfillment of the requirements for the degree of

          Masters of Applied Science

complies with the regulations of the University and meets the accepted standards with
respect to originality and quality.

Signed by the final examining committee:

                    Dr. Lyes Kadem   Chair

                    Dr. Narayanswamy Sivakumar   Examiner

                    Dr. Ashutosh Bagchi   Examiner

                    Dr. Muthukumaran Packirisamy   Supervisor

Approved by   _____
                 Chair of Department or Graduate Program Director

                 _____
                 Dean of Faculty

Date   _____

Abstract

Study on Optical Properties and Biocompatibility of Different Polymer-Gold Nano-composites
Platforms for Opto-Micro-Fluidic Applications

Michael Fanous

Microfluidic and microphotonic devices have become increasingly effective for diagnostic, clinical, and biochemical applications. Such technologies usually contain polymer materials, as their properties make them highly desirable for sensing possibilities. A useful addition to these materials are gold nanoparticles (GNP), which hold unique localized surface plasmon resonance (LSPR) properties that are affected by their structure, shape, distribution, and their degree of penetration into the surrounding medium. These characteristics, in turn, depend on the thermal history of the sample, that is, the extent and duration of heating of the polymer-GNP systems.

In this undertaking, thermally tunable gold-polymer nanocomposite platforms, which have customizable properties, are fabricated for emerging opto-fluidic applications. This is achieved using a thermal convection method using six polymer films: poly (vinyl alcohol) (PVA), SU-82, poly (styrene) (PS), poly (dimethyl siloxane) (PDMS), cyclic olefin copolymer (COC), poly (methyl methacrylate) (PMMA). In order to increase the plasmonic sensitivity of the platforms, the nanocomposites are, subsequently, subjected to heat treatment with incremental heating in the range of 80-200^{0}C. It is found that, among the polymers studied in this work, PVA and SU-82 show the largest shift of the Au LSPR band upon incremental heating as well as the highest plasmonic sensitivity. To test the biocompatibility of these different polymers, tagged antibodies are immobilized on the functionalized polymer films, and then the corresponding antigens are allowed to interact with the antibodies. The results of this work will be helpful in selecting a suitable material for both microfluidic and microphotonic experiments.

Acknowledgements

I would like to convey my gratitude, first and foremost, to my advisor Professor Muthukumaran Packirisamy for engaging me in his stimulating and first-rate Optical-Bio Microsystems group. I am honored to have worked under such an illustrious scientist, and for participating in a discipline with so many diverse and fascinating elements. Dr. Packirisamy has guided and mentored me throughout numerous exciting projects at the highest standards of academic research. I am confident that he has impressed on me his keen and exhaustive approach to achieving a commendable caliber of output.

Another person to whom I am immensely indebted is Dr. Simona Badilescu, the head supervisor in the lab. Dr. Badilescu has been instrumental at every milestone of my scientific progress. She has co-authored each of my papers and has been unfailingly patient and helpful with me throughout these seminal graduate years. Her formidable expertise and gumption have been indispensible to each undertaking.

I must also express my appreciation for the incessant assistance and camaraderie of all my colleagues in the Optical Bio-MEMS lab group, including Dr. Jayan Ozhi Kandathil, Durai Chelvan, Kiran Kuruvinashetti, Srinivas Bathini, Rahul Kumar, Mostapha Marzban, Jalal Abdul-Hadi, and Dr. Pierre Pottier.

Lastly, I would like to extend my thanks to those in my personal sphere of life who have provided me with much peripheral support in my academic activities, namely my mother, Stephanie Luetticken, my father, Dr. Nabil Fanous, and my sister, Dr. Amanda Fanous.

Contents

List of Figures

List of Tables

Nomenclature

AFM	Atomic Force Microscopy
COC	Cyclic Olefin Copolymer
FDTD	Finite-difference Time-domain
FTIR	Fourier Transform Infrared Spectroscopy
GNP	Gold nanoparticles
HIS	Hyperspectral Imaging Spectroscopy
LSPR	Localized Surface Plasmon Resonance
MPTMS	(3-mercaptopropyl) trimethoxysilane
PDMS	Poly (dimethyl siloxane)
PMMA	Poly (methyl methacrylate)
PS	Poly (styrene)
PVA	Poly (vinyl alcohol)
SEM	Scanning Electron Microscopy
Tg	Glass Transition Temperature
Tm	Melting Temperature
XRD	X-ray Diffraction

Chapter 1

Introduction and Literature Review

1.1 Objective

The motivation for integrating optic, fluidic and plasmonic effects onto a single nanoscale platform, in conjunction with thermally manipulated gold-polymer composites, is driven by the need for more intricate and versatile microdevices. In this context, plasmons refer to the oscillations of delocalized electrons at a metal-dielectric interface. Such an objective also entails the desire for greater material diversity, in order to address a specific purpose with the greatest material suitability. The forthcoming phase of biomedical devices will demand considerable enhancements in terms of detection and accuracy, and will have to fulfill the increasingly taxing goals for advancing medical, viral and bacterial sensitivity and treatment. Sensitivity here refers to the capability to detect an analyte at very low levels of concentration. Another aspect that the next generation of nano-biomedical devices should include is the ability to involve multiple elements in a highly sophisticated relationship, a constructive arrangement known as the multiplex system. This configuration enables the probing and processing of a horde of bio entities, yielding significant amounts of useful information, which leads to an improved understanding and treatment of various conditions [1].

The concept of miniaturization of an entire platform, and incorporating numerous functionalities onto a smaller working space, entails not only greater economy of dimension, but also an improved performance. Reducing the level of complexity of physical parameters, whether integrated in the device or external to it, has proven to yield more successful output [1].
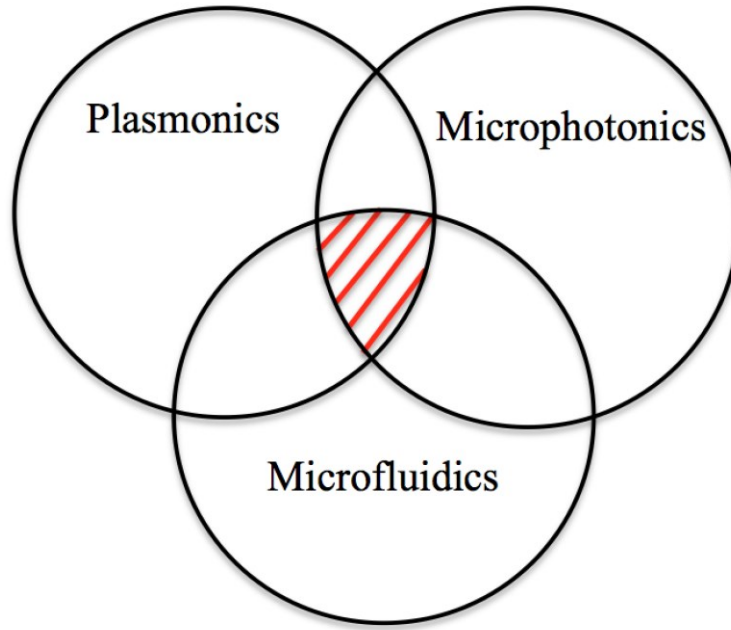
Figure 1.1 Scheme illustrating research intersection of opto-plasmo fluidic endeavors.

The inclusion of microfluidic effects in microphotonic platforms avails the capability to design and configure highly dense photonic devices. This combination benefits from three properties of fluids that are useful at the dimension of micrometers, which are a controllable movement, a considerable range of index, and sharp transitions of medium [2]. The examination of liquids, gases and plasmas using photonics is well established, but to involve fluids as utility components in the actual platform of the optical device is a fairly novel endeavor, though challenging in many aspects, such as fabrication difficulties. This integration is helpful in meeting the needs of constructing devices that involve fluids and optics [3].

Over the past decade, optofluidics has developed into a fertile and quickly expanding area for nanoresearch. It can be regarded as simply the generic combination of photonics and fluidics, a system or platform incorporating both phenomena, or it can refer to a class of miniaturized applications involving multiple functions on a single platform, such as the lab-on-a-chip technology. The uniform concept is to enable the direction and use of diverse fluidic and photonic elements in a variety of arrangements. The central novelty and source of innovation is the effective integration of optical elements such as waveguides and fibers, with liquid or gaseous media [3].

The entire realm of optofluidics was born out of the ambition to achieve a useful integration of fluids in photonics, for example fibers containing fluids for long-haul transmissions. Such furtherance has been fueled chiefly by the progress in microfluidics and the growth in multidisciplinary invention and application of photonic elements in the fields of medicine, biology and chemistry [3]. A significant initial desire for developments in optofluidics was the prospect to utilize fluidic devices and arrangements for photonic signal manipulation and transmission [3].

Optofluidics has since yielded a number of unprecedented features for medical and chemical technologies, especially in terms of particle detection and maneuvering, which may be suited for a number of purposes, such as sorting of cells and flow cytometers [3]. One example of a plasmon-opto-fluidic device is optofluidic systems that involve plasmonic waves and detect the level of photothermal conversion of gold nanostructures. The structure comprises a diode laser, a plasmonic system in water for photothermal conversion, and glass for gauging changes of the suspension [4].

1.2 Microfluidics

Microfluidics is a branch of science that involves the precise manipulation of fluids at the microscopic level. It is a technology that emerged in the early 1980s and was initially designed to develop ink jet printing and various devices in biotechnology. As a result of the continuing scientific advancements over the years, many other devices at this scale are now feasible, including valves, fluid mixers and micro-channels, which are used to move and maneuver fluids within a small chip. This feature has notably enhanced the possibilities of the lab-on-a-chip device, which may incorporate numerous laboratory procedures on a tiny platform, all at the dimensions of a few millimeters [5].

In terms of biological contributions, microfluidics can provide a means of delivering a high throughput of diverse cells in a cell-culture system that enables the close examination of cells and their interactions [6]. An example of this involves a chip paired with a 'laser guided cell-

micro-patterning system,' where optical forces help place separate cells into specific arrays [4]. The channel description of such a device is shown in Figure 1.2.
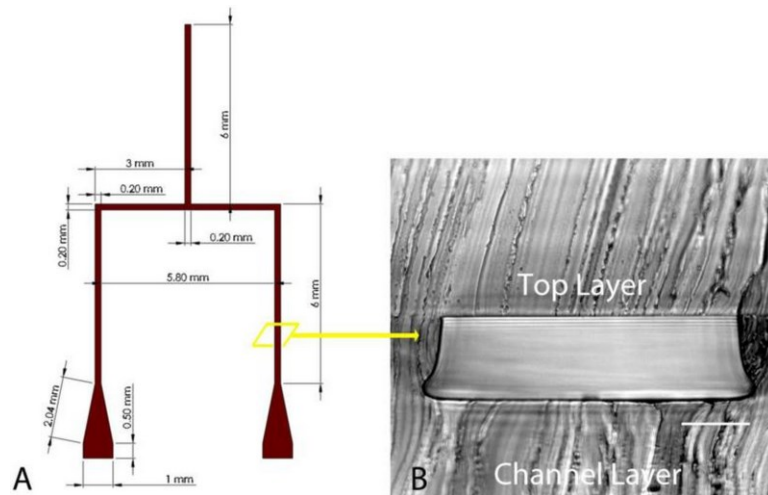
Figure 1.2 A) two-dimensional diagram of the microfluidic biochip flow-channel layer. B) a phase contrast image of a micro-channel cross-section. Scale bar 50 μm [6].

1.3 Microphotonics

Microphotonics is a type of technology that features the use of light in a microscopic system. In the same way that electronics was miniaturized to develop microelectronics, microphotonics has emerged from the effort to implement many optical functionalities onto a single chip [5]. One of the many possible devices in this field is a waveguide, as shown in Figure 1.3, which is a structure that transmits electromagnetic waves. Waveguides can differ in terms of shape and complexity, and may comprise other mechanisms, such as ring resonators [7].
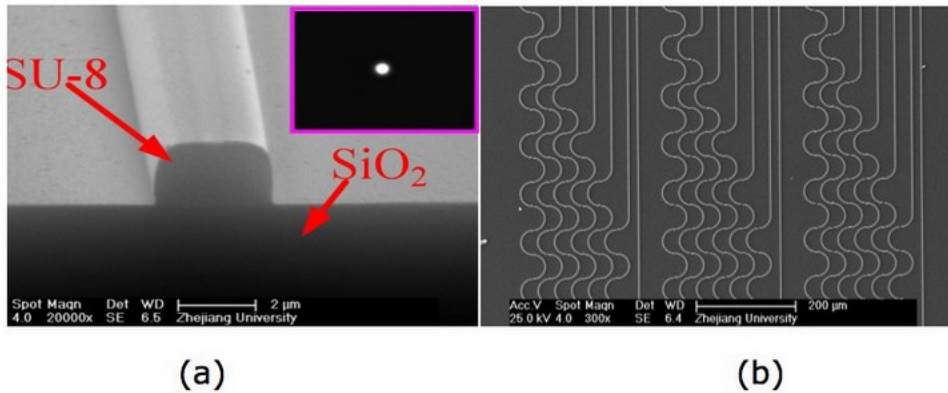
Figure 1.3 (a) SEM image of a small SU-8 ridge waveguide at the cross-section. (inset) Mode profile of the same waveguide. SiO2: silicon dioxide; (b) Bend array [7].

An example of a microscopic optical device that works alongside fluids is a waveguide that is employed for infrared wavelength transmission and convergence. It involves focusing light into fluid filled compartments for the purpose of cooling a lining of clothing. It is designed to be embedded in the fabric and take effect upon exposure to light [8]. Microchannels of 10 μm x10 μm were fabricated using interferometric lithography, as shown in Figure 1.4.
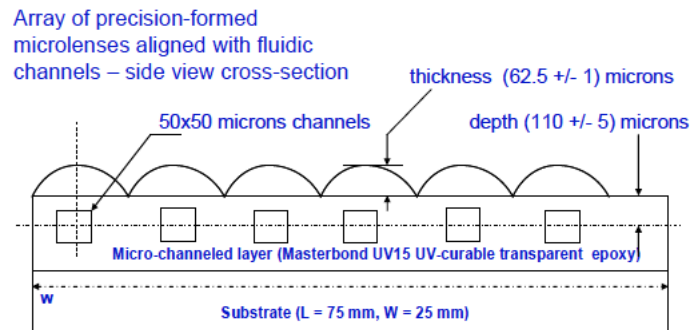
Figure 1.4 Technical drawing of the cross section fabric waveguide for heat removal [8]. The upper layer has an optimized curvature to focus the light into the rectangular compartments, as shown in Figure 1.5.

5
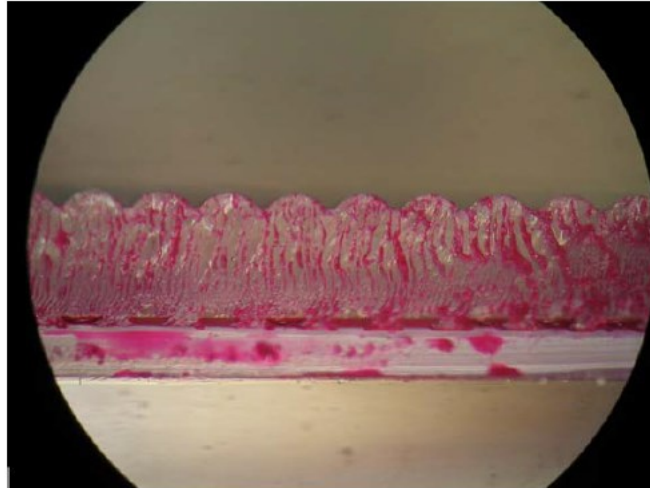
Figure 1.5 Microphotograph of the prototype of the waveguide embedded structure, using NOA73 adhesive [8].

Another important application of the waveguide is for sensing. An example is a chalcogenide sensing unit, in which monolithic waveguides are made on silicon wafers, as shown in Figure 1.6. The waveguides in this case have a large discrepancy in index and a low transmission loss of 2.3 dB/cm. A substance that is to be detected is injected into the microfluidic channel with a waveguide at the base. Sensing is calibrated by checking the optical output and measuring this against known spectroscopic values [9].
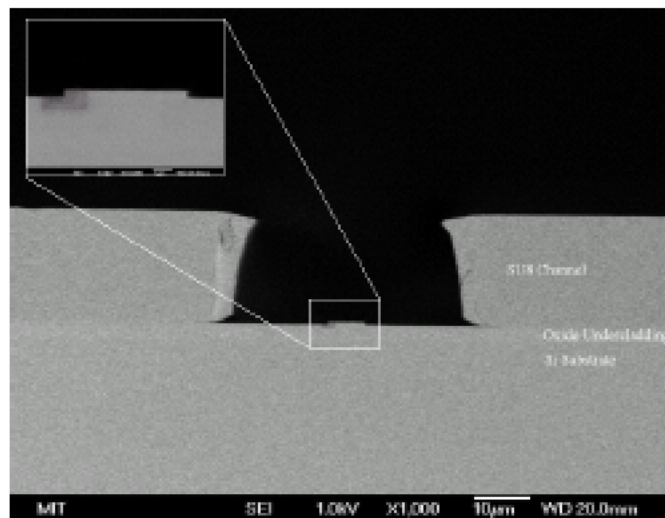
Figure 1.6 SEM image of 50 μm wide microfluidic channel and waveguide inside (inset) [9].

Combining these effects with microfluidics yields the possibility of even greater precision, miniaturization, sensing and functionality, and comprises the technology termed 'optofluidics.'[5]. Such devices include tunable attenuators, optofluidic lasers, and light sources, tunable filters, optical switches, and tunable interferometers [5]. An example of a highly multipurpose chip is depicted in Figure 1.7.
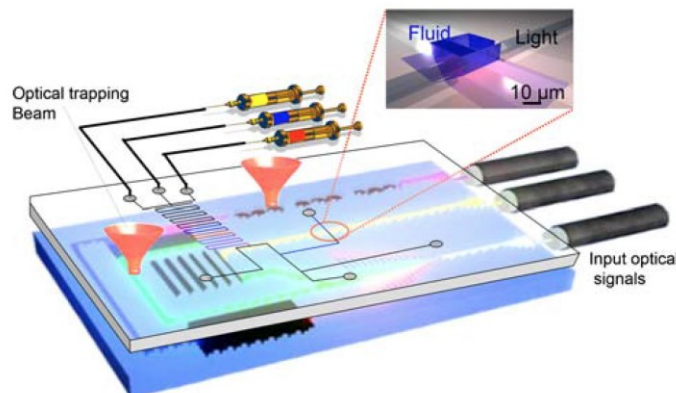
Figure 1.7 Depiction of a chip integrating light and fluids. The chip includes a photonic chip (bottom) that is paired with optical fibers, and a microfluidic circuit (top) [5].

1.4 Plasmofluidics

Surface plasmons (SPs) are coherent delocalized oscillations of electrons at the juncture of dielectrics and metals. Plasmonics is the branch of technology involving their analysis and use [10]. SPs have the capacity to influence light on the scale of nanometers, which entails a number of unusual and valuable effects, including localized heating and plasmon-induced transparency [10].

Another instance of their application employs the excitation of surface plasmons to detect biomolecules at the surface of metals. These are called surface plasmon resonance (SPR) sensors, and have been effectively produced to investigate the properties of fine molecular binding events [12]. Such technologies can be used to study chemical interactions with excellent sensitivity, enough to discern individual molecular activity. The missing element is the ability to precisely maneuver the analyte in question [13]. Microfluidic possibilities can compensate for this

deficiency with a considerable throughput of fluids. Plasmofluidics is the symbiotic duality of plasmonics and microfluidics in various devices to bolster overall device capability. It enables inventive designs in many areas, including optical sensing, imaging, and spectroscopy [14].

One specific example of this makes use of optical tweezes, which involve laser beams that exert forces that can maneuver separate cells, organelles, and compounds with high precision. Over the last generation of technological advancements, combining this phenomenon with microfluidic systems to skillfully guide particles has become a popular formula for diverse biophysical applications [15].
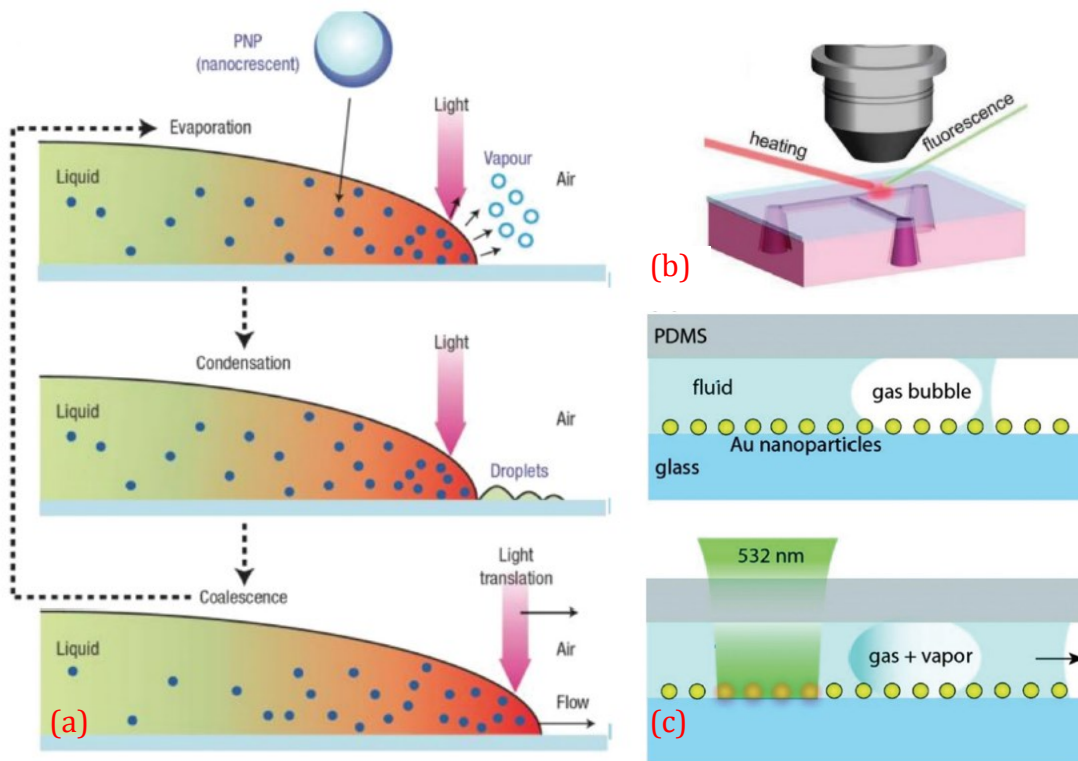
Figure 1.8 (a) Electromagnetically directed fluid flow using the plasmon-assisted photothermal procedure; (b) setup of phothermal application on PDMS pathways impregnated with gold nanoparticles; (c) separation and purification of microfluids through LSPR photothermal application on mass transitions using a gas bubble [16].

Another such incorporation was presented by Lui et al [16] in an endeavor that made use of plasmon photothermal effects of metal nanoparticles for the manipulation of fluids, as shown in

Figure 1.8 (a). Here, the nanoparticles in the fluid behave as localized supplies of heat, induced by the excitation of SPs. This leads to the vaporization of the fluid and the eventual condensation of droplets is utilized to control an overall movement of liquid. The precise control of the fluid may be performed with light beams of negligible intensity in conjunction with microfluidic grooves that help guide the liquid in a particular direction.

Metallic nanoparticles may be integrated with microfluidic channels. For instance, Fang et al [17] have devised PDMS channels impregnated with gold particles. A crisscross pathway made of the Au-PDMS nanocomposite, as shown in Figure 1.8 (b), was constructed and may be used to direct certain fluids with optical guidance [17].

Separation and purification of micro-fluids is feasible using intricate manipulation of flow by coupling the LSPR-enhanced photothermal phenomenon with a bubble transfer of mass [18]. A gas bubble is engendered and fixed to the fluid, as shown in Figure 1.8 (c), through photothermal influences on a surface bearing gold nanoparticles and PDMS microfluidic pathways. The division transpires as the laser beam impinging on the border of the bubble vaporizes the fluid and the gas condenses at the other end.

Another way surface plasmons may be used to supplement other conventional technologies is with a light trapping force. Although customary optical tweezers, which comprise focused laser beams to hold and move microscopic objects, offer many benefits, such as a noninvasive method of handling small items, they require expensive and cumbersome machinery. Plasmonic tweezers, which employ the sub-wavelength localization of near-field surface plasmons, are optimal for maneuvering particles with relatively minimal laser intensity.

Another effective manner of capturing nanoparticles is through plasmonic nanoantennas, which are coupled metallic nanoconfigurations with minute intervals between them that underpin markedly compact LSPRs. This possibility of controlling particles within short gaps has also contributed to plasmon-enhanced optical spectroscopy [19]. In pairing plasmonic trapping with electromagnetic molecular fixations, Galloway et al. [19] effectively manipulated gold nanocolloids, as shown in Figure 1.9, at certain areas of the antennas for spectroscopic endeavors.
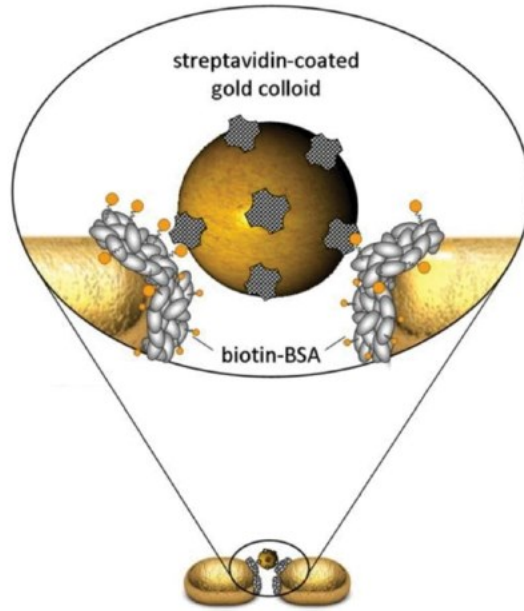
Figure 1.9 Illustrations of an individual gold nanocolloid adhering to a fixed protein in the interval of a gold dimer [19].

Another advancement in this field is the optical ordering of gold nanoparticles of dissimilar diameters in fluids. This was achieved by employing two crossing evanescent waves, which are waves that decay exponentially from their boundary, of dissimilar wavelengths directed at the junction between the underlying material and the fluid. By controlling the LSPRs of the particles within surrounding fluids, a number of plasmofluidic devices have been be realized

Another combination involves this effect with optics. Electronic circuits enable the manipulation of electron movement and the possible of their storage. Despite this, the effectiveness of electronic circuitry is proving increasingly unsuitable for transmitting signals across a certain distance. Optical resources solve this difficulty through photonic related technologies of fibers and circuitry. One way to minimize the dimensions of such technologies is to benefit from electronics and photonics effects by the use of surface plasmons [3]. Plasmonics provides many of the benefits of photonics and has the tenability of electronics. Surface plasmons allows one to scale light at the level of nanometers, as they are collective oscillations of electrons from light waves along the interface between a metal and a dielectric material [3].

The resonance between oscillations of electron densities at the interface of the metal and the electromagnetic field creates the surface plasmons, which are secured to the metal with rapidly diminishing fields in both adjoining environments. The decay length of surface plasmons into the metal is related to the surface layer depth. This characteristic of surface plasmons facilitates the direction of light in metallic structures of subwavelength dimensions, and it can be used to build miniaturized optoelectronic chips with nanoscopic elements. These kinds of devices can include other parts, such as waveguides, connection devices, controls, and mechanical couplers [3].

1.5 Polymers

Since the 1990s, glass has been the principle material for lab-on-a-chip substrates. Their properties, fabrication processes and applications were common as a consequence of the flourishing semiconductor and chromatography industry. For microfluidic technologies, however, the cost for diminutive items provided a stimulus (motivation) for the search of more economical alternatives, such as plastics. Polymers can be produced at considerably reduced costs, with simpler fabrication procedures and with a greater breadth of properties [20]. Microfluidic platforms are developing rapidly in their novelty and efficiency and the relevance of plastics in this enterprise is indisputably high. Plastics have become very sought after as a result of their economical accessibility, a practical alternative to glass, which is comparatively limited in terms of fabrication methods [21].

And since nanomaterials are becoming increasingly effective for various enterprises, they are being investigated more and more for their scientific possibilities. They can be exploited in a number of fields involving sensing, magnetism, electronics, and biomedical technologies. The combination of particles with established materials has brought about multifarious potential and is subject to progressively thorough experimentation. There is a sizable demand for specific materials that suit certain applications [22]. Involving microfluidics with the particle embedded materials has proven immensely successful as the flexibility in dimension and distribution cater to so many different configurations, enabling considerable optimizations [22].

The glass transition temperature (Tg) is the temperature at which a polymer film changes from a strong glossy material to a malleable one. If a polymer assumes a softer consistency when

exposed to an environment above its Tg, it is a thermoplastic. Thermoplastics are not affected chemically or dimensionally for a certain range of temperature above Tg [23]. This changeability in the material's properties with the introduction of heat may be harnessed to develop highly specific substrates for microfluidic or microphotonic applications.

PMMA was attractive from the early stages of material optimization as a result of its availability in numerous grades and its high optical transmission in the visible wavelengths. Recently, cyclic olefin copolymer (COC) has received attention for its optical clarity in the UV spectrum, as well as its low water permeability and considerable resistance to solvents [23].

Gold nanoparticles affected by localized Plasmon resonance may be regarded as tiny light-controllable sites of heat emission. The capacity to manipulate heat at the nanoscopic scale has many beneficial consequences for chemical, biomedical, and material possibilities. This phenomenon leads to a host of new potential applications involving the direction of fluid movement in microfluidic platforms on the dimension of nanometers [4].

1.6 Selection Rationale

The practice of minimizing the dimensions of microfluidic devices that analyze chemical and biological entities results in a more expeditious and economical system, and produces less waste. One essential component of such devices is the material that is used, which must be workable in terms of the environment that the machine is surrounded by, and the chemical and biological items that interact with the system. Additionally, the fabrication process must exhibit compatibility with the material of choice [24].

The polymers involved in this work have been chosen based on their dissimilar range of properties. Such dissimilarities have been classified and tabulated in Table I. In addition to their disparities in basic optical and thermal characteristics, there are properties that make each polymer unique and desirable.

SU-8 is a popular choice of material for microfabrication. It has fair stability at high temperatures and is not easily affected by moisture or solvents. This entails that the polymer will not distend or disintegrate in solvent exposing environments [25]. It has promising usage with highly dielectric materials. This is due to the considerable breakdown values of SU-8 that can heighten the net storage of electrical energy in nanocomposites [26]. Cyclic olefin copolymer (COC) is a constructive material for the platforms of microfluidic designs. They have considerable resistance to chemicals, a low absorption of water, and adequately transmit wavelength in the UV range [24].

COC has considerable temperature stability below 100°C and relatively low transmission percentages, which could be accounted by surface and bulk flaws causing scattering. These imperfections are more prominent in COC than in PDMS. PDMS differs however from COC in that it is an elastomeric polymer that has very good adhesion to a great number of materials. In terms of applications, it can envelop microchannels with removable seals [27].

PDMS is a very well known polymer in conjunction with the soft lithography process as a result of its simplicity to fabricate. Its characteristics include a larger permeability of O_2 and CO_2 than of most other polymers. As well, it exhibits high optical transmission from the UV range to the near infrared, which has many potential applications [24]. It is also suitable for biological implementations, as PDMS-based microfluidic systems have been used for cell manipulation and cytometric endeavors [28]. Additionally, PDMS nanowell platforms have been successfully undertaken [29], as well as PDMS bioreactor channels with fixed enzymes for biocatalysis assignments [29].

PMMA, which is a harder polymer, can be favorable in pursuit of a network without much flexibility. Their suitability must also be accounted for in terms of a lack of stability with organic solutions [24]. PMMA is a very accessible material, with pricing in the range of 0.2-2 cent per cm^2. It is also relatively malleable as a substance, with a molding pressure in the extent of 3.4 - 13.8 10^7 Pa. It is fairly hard and has excellent reproducibility for devices, similar to Polystyrene (PS) [20]. PS is the conventional option for drug investigation in cell-culture dishes and microtiter plates. PS is transparent, bio-friendly, chemically inactive, inflexible, and can be made hydrophilic by means of gas plasma and irradiation.

TABLE I. SELECTED AND OTHER POLYMER PROPERTIES

Polymer	Acronym	T_g (°C)	T_m(°C)	Solvent Resistance	Refractive index	Optical transmissivity (visible: 400 nm– 700 nm)
Cyclic olefin copolymer	COC	134	190-320	Excellent	1.54	Excellent 91 %
Poly (methyl methacrylate	PMMA	100-122	250-260	Good	1.48	Excellent 92 %[23]
Poly (styrene)	PS	92 -100	240-260	poor	1.55-1.59	Excellent 88 % [30]
Poly (dimethyl siloxane)	PDMS	-125	-40	moderate	1.41	Excellent 98 %
Poly (vinyl alcohol)	PVA	88.1	209.6	poor	1.50	Excellent 98 % [31]
SU-82	N/A	50-60 (not cross linked)	82	good	1.67	Excellent 98 %
Poly (carbonate)	PC	145-148	260-270	good	1.585	Excellent 91% [32]
Poly (sulfone)	PSU	170-187	180-190	fair	1.633	Fair 50-70% [33]

T_g: Transition temperature

T_m: Melting temperature

1.7 Gold Nanoparticles

During the last decades, gold nanoparticles have widely been employed for sensing applications. The use of temperature to improve such endeavors has also been explored. It was found that with optical illumination, gold nanoparticles engender heat [34]. This lead to several exploitations, one of which was imaging proteins with gold nanoparticles in cells. The heating of gold nanoparticles has therefore been considered a possible source of improved sensitivity of the platforms [35].

The properties of a material's surface differ from those of its bulk volume as a result of split or tense bonds. The effect is especially marked in polymers, as the discrepancies at the surface are considerable. One of the affected mechanical properties is the glass transition temperature. Multiple examinations of temperature transitions on polymer surfaces by various groups discovered that the surface transition temperature differs from the bulk transition temperature [36]. In 2003, Teichroeb and Forrest [37] obtained images of embedded gold nanoparticles in a polystyrene surface using atomic force microscopy (AFM). The result indicated that there is a more malleable region of material at the surface, about 3-4 nm in thickness. This leads to the inference that there is a lower transition temperature at the surface compared to the bulk region. One expected outcome of heating is the penetration or sinking of a part of the nanoparticles into the polymer, foreseen to generate a spectral shift in LSPR. This is in part a consequence of the alteration of the dielectric environment neighboring the nanoparticles, which become more enveloped in the underlying polymer layer the further they sink [38].

Surface Plasmon Resonance absorption bands are influenced by a number of factors of the material involved, such as its dimensions, shape, distribution, and surrounding environment. These facets may be manipulated in favor of improving the sensing capabilities by spectroscopy [B5]. One use of this involved the adsorption of double-stranded DNA onto gold nano-islands, with the shift of the LSPR band being pronounced by binding gold nanoparticles of 12 nm diameter, onto the complementary single-stranded DNA [39]. The plasmon resonance may also be manipulated through the polarity of the environments concerned [40,41]. Another possible facet to be manipulated is the degree of aggregation of the particles. It was also found that ameliorations on the limit of detection through further defining of the resonance peak might be

accomplished by using nanorods rather than nanospheres [42].

The way that heating in advance is implemented involves the transition temperatures of the materials. Since it was shown that the polymer surface layer has a glass transition temperature that is less than the commensurate bulk value, during the heating of polymer layers with a deposit of gold nanoparticles within the temperature range of Tg, s<T<Tg, the nanoparticles sink into in the surface layer of the polymer by an extent proportional to duration and intensity of heating [43].

Resonance of gold nanospheres takes place in the visible spectral region, at roughly 520 nm, which is the source of the crimson hue of the nanoparticles in solution [44, 45] The maximum of the surface plasmon band is also affected by the alterations to the polymer-nanoparticle arrangement that transpire during the course of heat treatment. The refractive index of the surrounding medium has been found to provoke an important shift of the surface plasmon band, described by Mie theory [46].

Gold nanoparticles have also been utilized throughout history to exploit their vermilion color in glass [47,48]. Their remarkably low refractive index has also proven a very desirable property for applications such as biochemical sensing and detection. As well, gold nanoparticles exhibit increased absorption and light scattering when their dimensions are less than the wavelength of incident light [49].

Surface plasmons are electromagnetic waves transmitted across the juncture of metal and dielectric environments. Due to the sensitivity of this effect to a slight electromagnetic trigger, this phenomenon is constructively employed as a method of sensing label-free biological entities [1]. In a variation of this method, one can introduce nanoparticles to host the conduction electron oscillations induced by the incident light, and use this as a biosensing technique. Such technologies have developed into what is known as localized plasmon surface resonance (LSPR). The difference in principle is depicted in Figure 1.10. LSPR works by recording the wavelength at which an absorption of the incident light is caused by a certain resonant frequency that is associated with the dielectric environment. Such an approach has many benefits, including a

simple operating procedure, and the ability to modify a sample before and after measurement in order to assess a particular change in spectral output. Also, since only a portion of the absorbed energy of the incident light remains as light in the form of scattering, and the remainder is dissipated by Landau damping [1], there will be a transduction of light to heat. This local thermal source has many potential applications, for example in catalysis or phase transition [4].
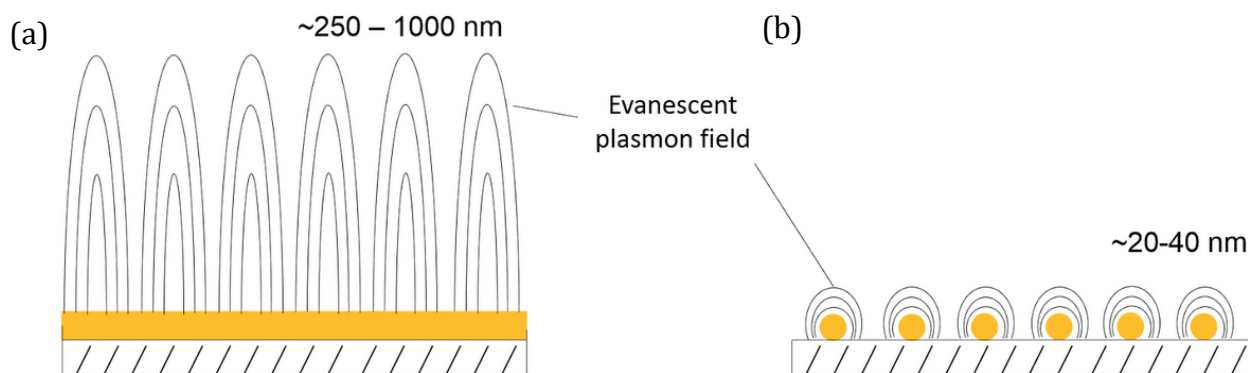
Figure 1.10 Schematic representing the difference between the principles of traditional SPR, (a), and LSPR, (b) [50].

1.8 Gold- polymer Nano-composites

The functional usages of these materials, whether made by in-situ or ex-situ synthesis, alone and in association with polymers largely involve their transparency in the Visible spectral range and most importantly, surface plasmon resonance and, in some cases, optical nonlinearity [51]. The combination of polymer and Au nanoparticles entails numerous areas of implementation, including electron and energy storage, and catalysis. In terms of medical applications, gold nanoparticles have high biocompatibility and can be paired to a multitude of biomolecular ligands, antibodies, and other biological entities, making them constructive agents for sensing and therapeutic applications. Colloidal gold nanoparticles are increasingly effective imaging elements due to their lack of cytotoxicity in immune-targeting [52], as well as their high resistance to photo bleaching or chemical disintegration [53]. They have been used successfully in cancer diagnosis and treatment, cancer cells imaging [54,55,56], and drug release [57]. The

capacity of gold nanoparticles to efficiently transform absorbed light into heat can be tapped for medical purposes, such as the photo thermal destruction of cancerous cells. Further, Loo et al [58] have achieved imaging, in unison with therapy, of breast cancers in vitro employing silica-gold nano-shells tethered to anti-Her2 antibodies.

The combination of polymers with metals results in a number of transitions in property. These changes are influenced by the size, shape and distribution of particles. Enlarging the particle diameter, for example, leads to absorption maximums of higher wavelengths [56]. Additionally, once the particles assemble, forming aggregates, their surface plasmons are coupled to produce extinction bands at longer wavelengths [59].

Another property of gold nanoparticles that must be accounted for is their high surface energy. Agglomeration of inorganic particles is promoted by their high surface energies, which generally exert up to 500-2000 mJ/m^2 in comparison with 20-50 mJ/m^2 for polymers [49]. This property, in combination with a heated polymer that undergoes softening, will lead to particles being submerged by the polymer to diminish their surface energies, resembling an 'embedding' effect. The arrangement of these polymer-embedded particles induces various property changes. The degree that the particles are lodged, their order, the depths and spacing of their immobilization – these parameters cause a specific dielectric environment, which in turn affects the electronic and optical responses of the hybrid material [60].

Nanocomposites can be fabricated in a number of different ways, particularly classified by either *in-situ* or *ex-situ* synthesis. The *in-situ* approach to forming nanoparticles in a polymer structure is straightforward and reliable. It is a very convenient way to produce an effective nanocomposite. It generally entails a single reaction that yields the nanoparticles from certain reactants, the precursors. This differs from *ex-situ* approaches in that the particles are synthesized within the polymer. There are many pros to this method, including a roughly uniform spacing within the polymer, and the possibility of agglomeration is prevented [61]. One undesirable possibility however is that the remaining starting reactants of the procedure may affect the characteristics of the resulting product [61].

The *in-situ* approach to forming the nanocomposite involves engendering the particles from within the polymer material through a chemical reaction. A different approach would be to obtain a commercial preparation of a GNP solution. A difficulty then arises in the endeavor to fix the nanoparticles to a polymer surface, since some polymers like PDMS exhibit poor adhering properties for particles. A solution to this was found to be the initial application of 3-aminopropyltriethoxysilane (γ-APTES) (Trung et al. 2012) [62]. When nanoparticles are formed inside a microfluidic setting, it predominately involves the blending of fluids to bring about a chemical change. This can be performed using a steady flow throughout the microfluidic channel or by droplets [62].

The *ex-situ* approach, on the other hand, which is still an effective method for the composite preparation, involves combining pre-made nanoparticles with the polymer network in an effort to make a composite.

This type of synthesis is convenient when considerable amounts of the product are needed for industrial purposes, and larger, less specific implementations. The difficulty with the process involves the adequate synthesis of nanoparticle before integration with the polymer material, which are prone to agglomeration and failing to adhere to the surface of the polymer. This is because the particles are only fixed to the polymer by means of physisorption, a phenomenon that does not comprise a chemical change, but only has a physical bind [61]. The *in-situ* change or reaction can happen at the edges or with the bulk of the polymer material, where part of the polymer structure decelerates the process [62].

Because of the low chemical potential of Au, ions can be easily reduced in the presence of even weak reducing agents. One method to achieve gold nanoparticles embedded in the surface of a polymer involves *in situ* reduction of $HAuCl_4$ inside a thin polymer film, leading to the formation of gold nanoparticles of various shapes [63]. Many groups developed gold-polymer nano-composites through *in situ* methods and built sensing platforms based on the gold Localized Surface Plasmon Resonance (LSPR) band [63]. Other techniques involve functionalizing a polymer (in this case PVA) with (3-mercaptopropyl) trimethoxysilane (MPTMS) producing a thiol functionality on its surface. Thereafter, gold particles are embedded

on the surface of partially dried functionalized PVA, whereupon the gold particles are chemisorbed onto the thiol groups [56]. A polymer and precursor can also be first mixed in a common solvent and immediately thereafter, the nanocomposite film is formed by evaporation of the solvent [60]. In another process, to generate silver nanoparticles in a polymer, Porel et al [64] carried out an *in situ* fabrication, using an aqueous solution of silver nitrate and PVA for the fabrication of a free-standing film. In this case, PVA serves as both a reducing agent of the nanoparticles and as the host for uniform dispersion and suspension.

The effect of heating on a gold - polymer nanocomposite film has previously been investigated. For example, Liu showed that heating a composite at 90℃ caused the gold particles to become entirely enveloped by the polymer material (in this case PMMA). In this work, it was thought that the formation of the composite was facilitated at the glass transition temperature (Tg) of the gold-PMMA composite [57]. The new viscous state of the polymer surface induces a flow around the nanoparticle and adsorbs onto the nanoparticles' surface, decreasing their surface energy [65].

Generally, it has been confirmed experimentally that heating gold aggregates at 400-500^{0}C, provoked a blue-shift and a narrowing of the Au LSPR band, with a beneficial effect on sensing. However, to the best of our knowledge, the behavior of gold-polymer surface nano-composites under incremental heat treatment at lower temperatures has not been reported. Our preliminary results have shown a large red-shift of the Au LSPR band when surface nano-composites were heated incrementally and, to describe this technique, we coined the term of `thermal manipulation`.

Herein we report a detailed analysis of thermal manipulation of Au-particles embedded in polymers that varies from previous development and examination of this phenomenon in various respects. In this work, the nanocomposites are subjected to systematic heating that enables investigation of the material at different stages of heat treatment, both at the cross-section and on the surface of the composite material. The convective method of evaporating a gold colloidal solution onto the polymer films is novel for this type of experiment, and allows for the gradual

evaluation of particle penetration from the surface to the bottom of the film. The sensitivity and other composite properties are measured for six different surface nano-composites.

1.9 Proteins

Understanding the interactions between a polymer surface and proteins is important information for the development of microdevices. The quality, the topography of the surface, etc. are parameters that ultimately will determine the amount the homogeneity of the walls, and the amount of adsorbed proteins. Model polymer systems, that is, polymers designed for future applications in microfluidics, are investigated in this work. As the adsorption of proteins by a polymer substrate is usually a precursor step to the attachment of cells, the biocompatibility of polymers in this work is evaluated by detection of a fluorescent antibody.
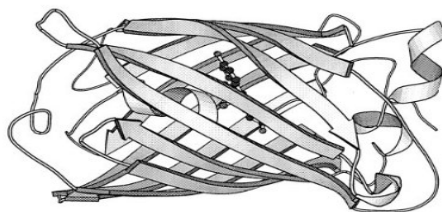
Figure 1.11 Green fluorescent protein structure [6].

Another imperative to examine the biocompability of polymers is that in terms of materials for microfluidic devices, polymers overall are more favorable than glass. They diminish the expense and facilitate the manufacturing process. Furthermore, the multifarious types of polymers enable greater choice for materials that are suitable for specific applications [67].

In addition to the adsorption of analytes, complementary research may include the assessment of other relevant properties for microfluidic designs. As electroososmotic pumping is used to propagate flow in microfluidic designs, the electrical insulation of the material is of paramount importance to ensure that the electric field will be applied across the fluidic channel. Polymers also offer more possibilities for sealing the microchannels, as opposed to glass [67, 68].

The other critical properties of materials involved in microfluidic products include the transition temperature, the melting temperature, water absorption, solvent resistance, and optical transmissivity [69].

The assessment of biocompability may also be constructive information for research regarding other medical applications of polymers, such as the growth of cell sheets, tissue scaffolds, vaccination, and the treatment of genetic diseases [70].

1.10 Contributions: Publications, Presentations & Pending Submissions

1. Fanous, M., Ozhikandathil, J., Badilescu, S., and Packirisamy, M. Evaluation of Optical Properties and Biocompatibilty of Polymer Materials for Microfluidic Applications, 35832, proceedings IEEE Photonics North. Conference, Ottawa, Canada, June 9-11, 2015.

2. Fanous, M.,Badilescu, S., and Packirisamy, M. Thermal Manipulation on Localized Surface Plasmon Resonance Sensitivity of Polymer-Gold Nano-Composites, Photonics North. Conference, Quebec City, Canada, May 25, 2016.

3. Fanous, M.,Badilescu, S., and Packirisamy, M. Effect of Gradual Heating of Gold Nanoparticle Multilayers on Polymer Substrates on the Characteristics of their LSPR Bands, proceedings. Conference, ICNFA, NewTech'16.

4. Fanous, M.,Badilescu, S., and Packirisamy, M. Effect of Gradual Heating of Gold Nanoparticle Multilayers on Polymer Substrates on the Characteristics of their LSPR Bands. International Journal of Theoretical and Applied Nanotechnology (IJTAN). (Submitted on July 6, 2016, 8 pages, ID# 126, pending review).

5. Fanous, M.,Badilescu, S., and Packirisamy, M. Thermal Manipulation for Microfluidic Platform Optimization, Plasmonics. (Accepted on January 2, 2017).

6. Fanous, M.,Badilescu, S., and Packirisamy, M. (2016), Investigation of Thermal Manipulation on Polymer-Gold Nano-Composites with Raman Spectroscopy and Fourier Transform Infrared Spectroscopy (FTIR). (Under preparation).

7. Fanous, M, Badilescu, S., and Packirisamy, M. (2016), Investigation of Sensitivity of Polymer-Gold Nano-Composites in Mediums of Various Refractive Indices. (To be Submitted).

Chapter 2

Fabrication and Thermal Manipulation

The polymers examined in this work are poly (methyl methacrylate) (PMMA), poly (styrene) (PS), SU-82, poly (vinyl alcohol) (PVA), poly (dimethyl siloxane) (PDMS), and cyclic olefin copolymer (COC). The polymers were spin-coated on glass substrates and subsequently annealed for a time that is appropriate for its properties. Spin coating was undertaken with the following speeds and durations:

TABLE I. SPING COATING PARAMETERS

Polymer	First duration (seconds)	First speed (rpm)	Second duration (seconds)	Second speed (rpm)
PMMA	10	500	30	2500
PS	10	150	20	600
SU-82	10	500	30	2000
PVA	10	500	20	1000
PDMS	10	500	30	4000
COC	Polymer was purchased from TOPAS as film.			

2.1. Fabrication of Polymers

The solutions of the polymers were prepared by using a suitable solvent. For poly (styrene) a 5% solution was prepared in anhydrous toluene. Poly (vinyl alcohol) was dissolved in water to a concentration of 5 %. SU-82 was purchased as a liquid while PMMA (495 A11) was purchased as a solution. SU-82 is a type of negative photoresist that is epoxy-based. Cyclic Olefin Copolymer is a relatively new material that has shown to have unique optical properties and has been used in recent medical devices. It was purchased from TOPAS in a film form, which was practical in that no spin coating was required. The material was cut in dimensions of 1cm x 4 cm, in order to match the size of the glass slides.

PDMS was fabricated by first mixing a curing and base agent in a ratio of 1:10 in a small transparent container until the resulting mixture had a milky appearance. The mixture was then placed in a desiccator and the vacuum was turned on and off for short elapses, in order to expel the air from the mixture.

2.1.1 Operating Procedure for PDMS Fabrication

1. Container
    1.1.   Wash a 100 ml beaker with water and isopropyl alcohol.
    1.2.   Zero the beaker with a digital balance (Ohaus Scout Pro).
2. Substance Preparation
    2.1.   Pour an amount of the base agent (SYLGARD 184 SILICONE ELASTOMER BASE), in the range of a dozen grams (13.35 g), into the beaker.
    2.2.   Pour one-tenth this amount (1.335 g) of the curing agent (SYLGARD 184 SILICONE ELASTOMER CURING AGENT) into the beaker.
    2.3.   Blend the contents gently with a toothpick so as the render the mixture homogeneous.
3. Evacuation of bubbles
    3.1.   Place the beaker in a desiccator connected to a pump (Fischer technical company LAV-3).

Figure 2.1 PDMS Station.

    3.2.   Make the tubing airtight by rotating the lever of the valve crosswise, as shown in Figure 2.1.
4. Continuation of process

24

4.1.   Turn on the pump for a short elapse (30 seconds), then turn it off.

4.2.   Repeat step 4.1 while periodically checking the beaker until the mixture has no more bubbles.

Once obtained in liquid form, the solutions of the polymers were then spin-coated on glass substrates and thereupon annealed at a temperature and duration that is specified according to their properties. The films were kept in the oven for 2 hours at a temperature between 60°C and 80°C to remove the traces of solvent. Cyclic olefin copolymer was purchased from TOPAS in the form of a solid sheet.

Figure 12.2 Spin coating machine and dial.

2.1.2 Operating Procedure for Spin Coating

1. Preparation

    1.1.   Clean room

        1.1.1   Open the air valve for cleanroom operations.

        1.1.2   Put on all necessary cleanroom apparel.

    1.2.   Slide preparation

        1.2.1.   Wash a glass slide (1cm x 4 cm) with acetone.

        1.2.2.   Dry off with the air nozzle.

        1.2.3.   Wash the glass slide with isopropanol.

        1.2.4.   Dry off with the air nozzle.

    1.3.   Fixing the sample

1.3.1.　Open lid of the spin coating machine and clean the base with a Kimtech tissue.

1.3.2.　Line the lower portion around the suction column with aluminum foil.

1.3.3.　Place the center of a plastic disk over the suction aperture, after making certain it is clean and dry.

1.3.4.　Fix the slide to this platform by either attaching a loop of scotch-tape to its underside, or by fixing the edge of the slide with an adhesive.

2.　Depositing polymer

2.1.　Transfer a small quantity (3-4 ml) of the polymer to the middle of the slide by using a syringe.

2.2.　Depending on where the intended measurement will take place, spread the liquid polymer predominantly in that area.

2.3.　Close the lid.

3.　Running the spin process

3.1.　Press F1 on the dial and select speed settings according to the polymer's parameters.
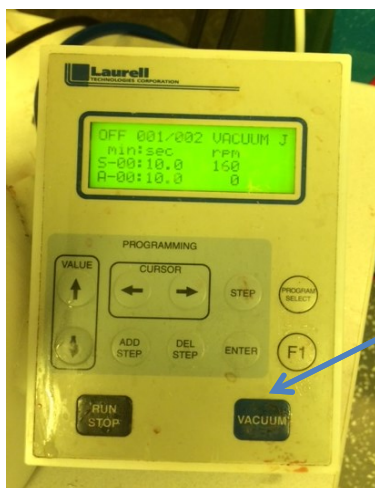
Figure 13 Spin coating dial.

3.2.　Turn on the pump.

3.3.　Begin spin coating by pressing start

4.　Cleaning afterwards

4.1.　Once the process comes to a stop, turn off the pump and retrieve the slide.

4.2.　Dispose of the adhesive and aluminum foil.

4.3.   Clean the plastic disk, the suction platform, and the inner surfaces should any polymer have leaked or splashed.

4.4.   Close the lid and clean the beaker.

5. Post-treatment of slides

5.1.   Place the slide/s into a clean petri dish and then put them in an open oven (Fischer Scientific Isotemp Oven) for a temperature and duration appropriate to their properties (65 °C for two hours).

5.2.   Transfer the slides to the fume hood (VAV/ vertical).

2.2. Fabrication of GNP

A gold colloidal solution was used to deposit gold nanoparticles on the polymer films through a thermal convection method. This technique involves the transfer of gold nanoparticles from the colloidal solution onto the polymer film through evaporation and assembly. Spherical gold nanoparticles were produced according to Turkevich's method [14], employing the reduction of chloroauric acid by sodium citrate. The solution was prepared from 1mM of gold(III) chloride trihydrate dissolved in 90 ml of water, which was subsequently boiled. 15 mL of a sodium citrate solution (2%) was added and the solution was heated until the color of the solution became red-purple. After that, the solution was further boiled for 15 min and then left to cool to room temperature.
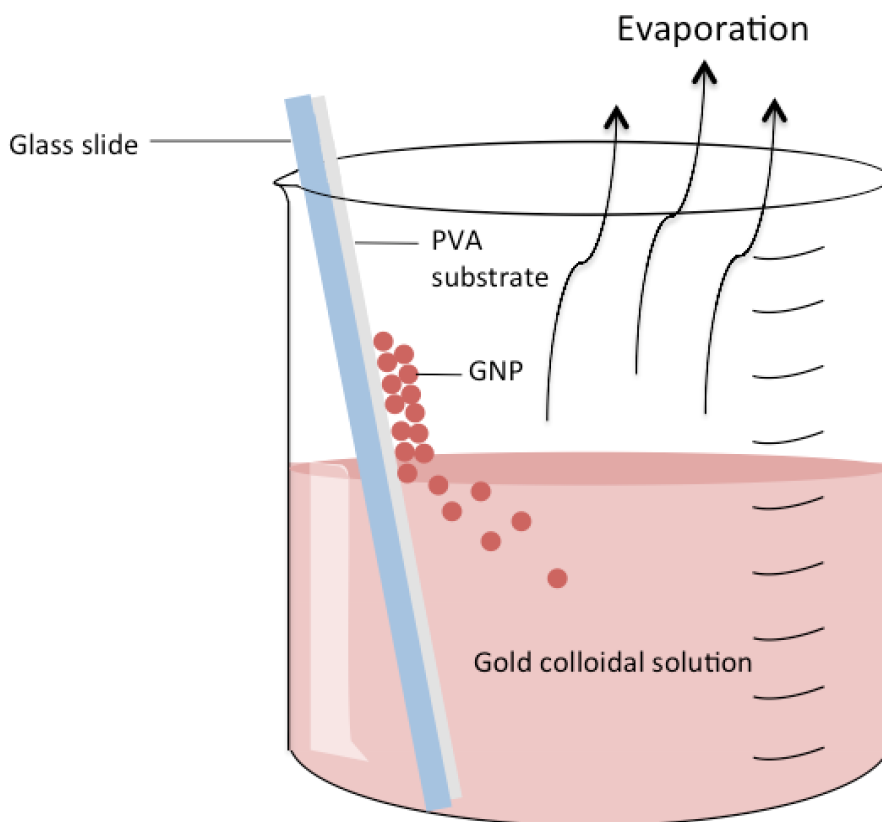
Figure 14 Schematic of the convective assembly procedure of deposition of gold nanoparticles.

The gold colloidal solution was evaporated onto the slanted (inclined, slightly angled) polymer samples in a beaker and the gold nanoparticles were self-assembled through a convective assembly process, as shown in Figure 2.4. Once immersed in the solution, the slides were kept in the oven until the whole amount of gold was transferred to the substrate, typically for a duration of two days.

2.2.1 Operating Procedure for Thermal Convection

1. Preparation
   1.1. Prepare the gold colloidal solution by obtaining 1mM of $HAuCl_4$ precursor or gold (III) chloride, 15ml of 1% sodium citrate sodium, and deionized water:
   1.2. Weigh 0.003 g of the gold precursor over a small hexagonal plastic plate on a digital balance (Denver Instrument SI-114) and transfer it using a laboratory scoop into a 100 ml beaker.

1.3.   Add 90 ml of DI water to the beaker.

1.4.   Prepare the sodium citrate solution by dissolving 1 g of sodium citrate in 100 ml of DI water in a volumetric flask using a funnel. Label.

1.5.   Mix the contents to achieve a uniform faint yellow hue.

2. Heating

2.1.   Place the beaker over a heating platform (Corning) in the fume hood, and set the temperature to 80-100 °C.

2.2.   Wait until the mixture boils, and then add 10 ml of sodium citrate to the beaker in a steady stream of droplets with a syringe.

2.3.   Observe a purple shade begin to appear and turn the heater off.

3. Erlenmeyer flask

3.1.   Wait for the beaker to cool and transfer contents to an Erlenmeyer flask in the fume hood.

4. Preserve

4.1.   Seal the opening by stretching a measure of parafilm wrap over the lip of the flask.
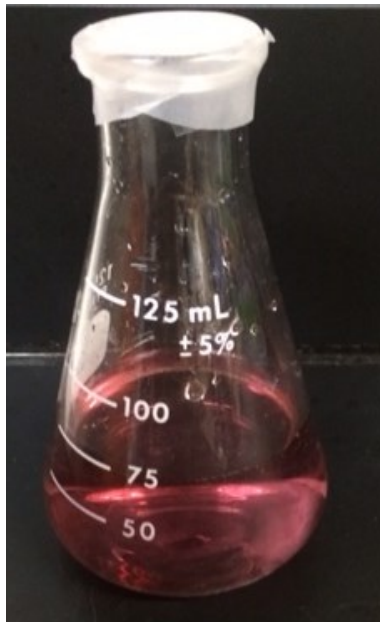
Figure 15 Erlenmeyer flask with gold colloidal solution before aluminum covering.

4.2.   Cover the flask entirely in aluminum foil in order to prevent any tampering of light. Label.

5. Slides

    5.1.   Place 1-4 numbers of polymer spin coated glass slide/s in the beaker, polymer facing upwards, leaning on the border and inclined at approximately 30 degrees, as shown in Figures 2.4 and 2.6.

Figure 16 Picture of a beaker with a polymer slide a kept at roughly 30 degrees, with scotch tape.

    5.2.   Fasten the upper edge of the slide to the rim of the beaker with scotch tape.

6. Thermal convection

    6.1.   Pour 40 ml of the gold colloidal solution in the beaker and place in the open oven.

    6.2.   Set the oven to 65 °C and leave for 2 -3 days.

7. Post-evaporation handling

    7.1.   Find the beaker dried, with the slides bearing a purplish border and the bottom half of the beaker tinted purple, as shown in Figure 2.7.
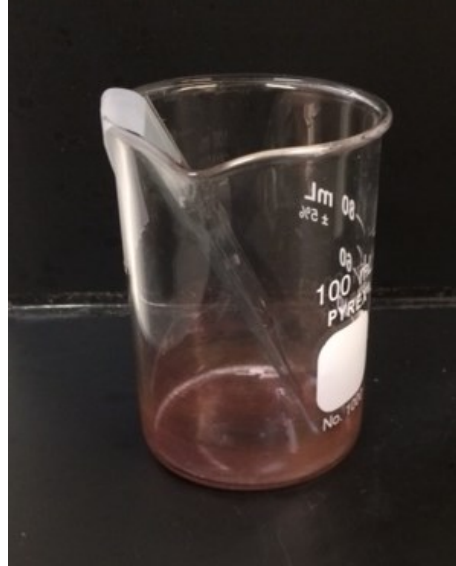
Figure 17 Beaker and slide with purplish hue.

7.2.   Place the slides in the fume hood until the time to proceed with measurements.

2.3.   Thermal Embedding of GNP for *ex-situ* integration

The polymer films, having the gold particles on their surface, were heated gradually, starting from 80^0C and increasing the temperature in increments of 25 °C for durations of 10 minutes each. This approach enables progressive measurements of the samples as they are being heated. The first temperature of heating is 80°C and after ten minutes, the slides are taken out of the oven and left to cool to room temperature, before recording the spectrum. They are subsequently placed in the oven at 100 °C for another ten minutes. This process is repeated at temperature increments of 25 °C, and the cycle is continued until right before the polymer's decomposition. A slide of PVA, heated directly at 200 °C for 30 minutes, was also used for comparison.
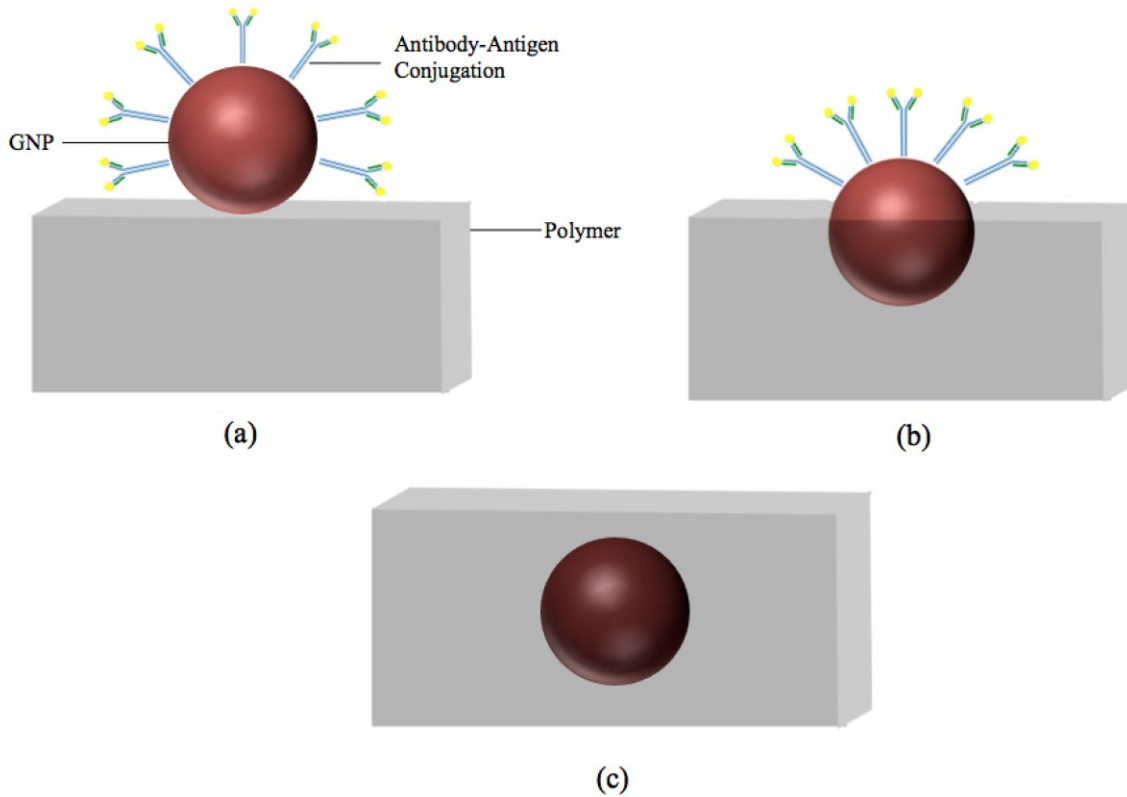
Figure 18 Schematic of different embedding possibilities: (a) no embedding; (b) partial embedding; (c) complete embedding.

This process, and the possible resulting effects, is depicted in Figure 2.8. Each scenario has its advantages and drawbacks. When the particle is only adhering to the surface of the polymer layer, a great deal of the particle may host antibodies or other biological specimens for detection. The greater surface area makes this suitable for sparse or low affinity entities. However, without a strong interface, the grip is unreliable and may be unstable or unsteady for sensing purposes. Additionally, the configuration has very few morphological options. Only the variable of surface arrangement can be controlled. Partial drive-in, on the other hand, ensures a more secure attachment to the polymer, and is amenable to multiple arrangements. Lastly, a complete embedding of the particle in the polymer material may induce desirable property changes, including enhanced elastic modulus and optical transmission differences but sensing would not be possible. This last step may also include particles still on the surface of the polymer. The exact details of such procedures involving heat for a number of relevant commercial polymer

materials should hence be of considerable interest to numerous contemporary scientific endeavors.
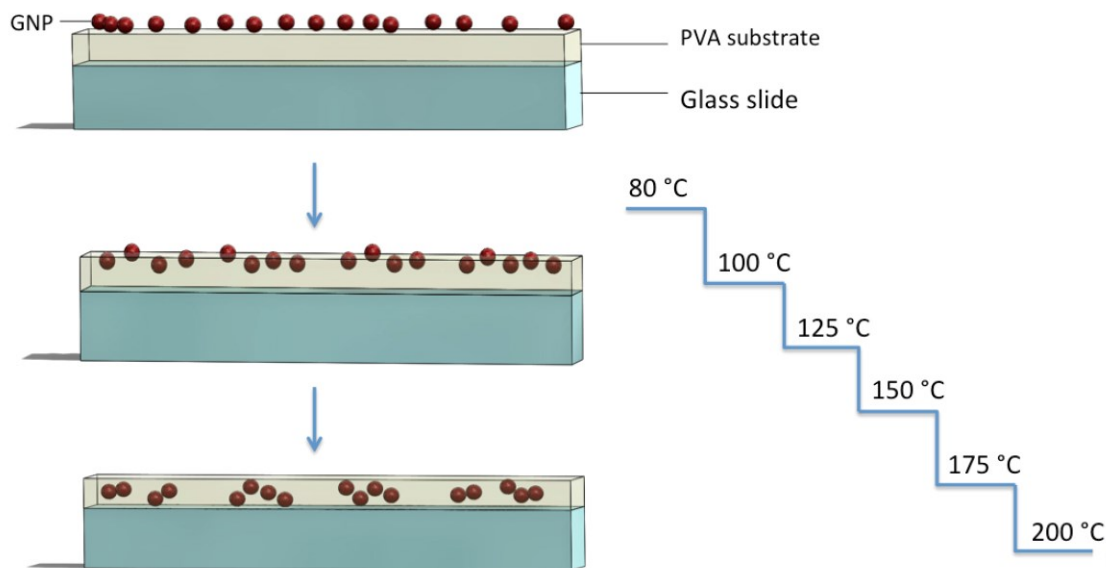
Figure 19 Schematic depicting the gradual morphological changes through incremental heat treatment of Au NPs – polymer nanocomposites.

2.3.1 Operating Procedure for Heat Treatment

1. Preparation
   1.1. Set a closed oven (Thermo Scientific Thermolyne) to 80 °C.
   1.2. Line the samples into a petri dish or onto an aluminum sheet and insert them into the pre-set oven for 10 minutes.
2. Step 1
   2.1. Remove the samples and set the oven to 100 °C.
   2.2. Wait five minutes for the slides to cool and proceed with any dry measurements (LSPR, Raman Spectroscopy).
3. Subsequent steps
   3.1. Place the slides into the pre-set oven.
   3.2. Repeat steps 2.1-2.2 with increasing temperature increments of 25 °C until the increment before the polymer's decomposition value.
4. Control Sample

4.1.   Pre-set the oven to 25°C below the sample's decomposition temperature.

4.2.   Heat the sample in the oven for 30 minutes.

Heat treatment has different consequences for different polymer substrates, a quality demonstrated in Table III, which lists the extent of possible thermal application with the aforementioned procedure. The yellow boxes indicate that the polymer underwent decomposition and was no longer usable. The approximate sign indicates that the polymer substrate had to undergo to multiple attempts due to difficulties after heating and obtaining consistent or usable results in terms of LSPR measurements.

TABLE III. POLYMER HEATING STEPS

Polymer	100 °C	125°C	150°C	175°C	200°C	225°C
COC	✓	✓	✓	✓	✕	
PS	✓	✓	✓	✓	✓	✓
PVA	✓	✓	✓	✓	✓	✕
PDMS	✓□~	✓□~	✓□~	✓□~	✓~	✓~
PMMA	✓□~	✓□~	✓□~	✓~	✓~	✓~

✓□workable temperature;   ~ multiple attempts needed; ✕ decomposition; yellow - decomposition

For measurements involving examinations of the cross-section of the samples, a diamond cutter was employed to incise across the deposited ends of the slides. A method used to quantify the sensitivities of the nanocomposite platforms involved immersing the slide in solvents of distinct refractive indices, such as ethanol and toluene, and measuring the LSPR shift between them and distilled water.

2.4. Biocompatibility Testing

For biocompatibility tests, a chemical linker was applied to the surface of the non-heated polymers, specifically, 1-octadecanethiol (NanoThinks 18), in order to consolidate the binding with the proteins. The protein, subsequently introduced in a droplet through a micropipette, was

the green fluorescent recombinant protein monoclonal antibody, in a phosphate buffered saline (100 µg/200 µL). These flurophores have an excitation wavelength of 395 nm, and an emission peak at 509 nm. This affinity of this substance was detected using spectroscopy techniques for all six polymers, producing a different band each time. The conjugate antigen solution to this is named GFP, AEQUOREA protein recombinant (Sino Biological – Life Technologies), and has been prepared by using 100 µg of it in 50 ml of the PBS solution. This solution, after the antibody had dried, was applied in droplets to the slide and spectroscopic measurements were again made. The resulting spectra could thus be juxtaposed to analyze the binding degrees of the GFP. The opposite process, wherein the antigen solution is first measured and then the antibody solution is later added, was also undertaken.

To summarize, the six materials included in this work are poly (methyl methacrylate) (PMMA), poly (styrene) (PS), SU-82, poly (vinyl alcohol) (PVA), poly (dimethyl siloxane) (PDMS), and cyclic olefin copolymer (COC). They were prepared as a liquid and developed over a glass slide as a film using the spin coating method and subsequent annealing. A novel thermal convection technique was employed to coat a layer of gold nanoparticles on the surface of the polymer slides. The resulting platforms then underwent a process of thermal tuning to bring about various patterns of GNP embedding and clustering.

Chapter 3

Test Methodologies

The methods employed to examine the interaction between the gold nanoparticles and the polymers are: UV-Visible spectroscopy (Pekin-Elmer's LAMBDA 650), Scanning Electron Microscopy (S-2499n model from HITACHI and Oxford Instruments), Atomic Force Microscopy (3100 AFM model), Raman spectroscopy using a 795nm laser, Fourier Transform Infrared Spectroscopy (FTIR), and Hyperspectral Microscopy (CytoViva).

Table IV indicates which polymers were tested with which method. The heated and non-heated versions of the slides are indicated by 'h' and 'n-h' respectively, and those with protein measurements are indicated with the acronym 'GFP' (green fluorescent proteins). If a cross-section measurement was made, it is indicated with 'cross.' If a control slide with no gold was recorded, it is shown with 'c', and the question mark represents measurements that were not taken because of feasibility or because the results were not reliable or accurate. A lack of accuracy could be because of coarseness, such as when the cross-section is being measured. When one endeavors to cut the glass slide, even a diamond cutter may yield severely corrugated edges at the micrometer level, defeating the purpose of microscopic investigations. It should also be noted that some materials are not compatible with certain methods, such as glass slides with FTIR, which is why only the COC slides were assessed with this method.

TABLE IV. METHODS AND POLYMERS OF MEASUREMENTS

Polymer Measured	XRD	SEM	AFM	H-M	LSPR	Sensitivity	Raman	FTIR
PDMS	?	h/ n-h/GFP	h	?	GFP/n/n-h/c	h	?	?
PS	?	h/GFP	h	?	GFP/n/n-h/c	h	h	?
PVA	h/ n-h	h/n-h/ GFP	Cross/ heated/ non-heated	h/n-h	GFP/n/n-h/c	h/n-h	h/n-h	?
COC	?	h/GFP	?	?	GFP/n/n-h/c	h	?	h/n-h/c
PMMA	?	h/n-h/GFP	h	?	GFP/n/n-h/c	h	n-h	?
SU-82	?	h/n-h/GFP	h/non	?	GFP/n/n-h/c	h	?	?

h: heated slides; n-h: non-heated slides; cross: cross section ; GFP: green fluorescent protein; c: no gold nanoparticles.

3.1. Scanning Electron Microscopy (SEM) and Atomic Force Microscopy (AFM)

SEM and AFM were utilized both to image the surface of the slides, to discern the distribution of particles, and at the cross section of cut edges, to investigate the depth of particle embedding. Some samples were coated with 70% gold and 30% palladium to enhance the conductivity and facilitate detection of particle outlines. The parameters for the SEM measurements are shown in Table V.

TABLE V. SEM PARAMETERS

Measured polymer	Number of areas/ purpose	Magnification/ variable pressure	Aperture (mm)/ probe current (mA)	Accelerating voltage/ Working distance
PVA	5 /GFP	Low-high/60Pa	4/low-high	2kV-10kV/ 7.5
	13/GNP	3;5;10 μm/ 60 Pa	4/50	15kV/7.5
COC	1/GFP	Low-high/60Pa	4/25-30	2kV-10kV
SU-82	9/GFP	40;50;70k/60 Pa	4/25-30	2kV-10kV/ 7.5
PMMA	6/GFP	40;50;70k/60 Pa	4/25-30	2kV-10kV/ 7.5
PDMS	12/GNP	1;3;5 μm/60 Pa	4/50	15kV/7.5

3.2. Hyperspectral Microscopy

Lastly, a hyperspectral microscope was used, which has the capability to combine spectroscopy and imaging, focusing on individual particles or clusters for spectral analysis. This method enhances both the specificity and accuracy of the final spectral results, in addition to providing highly valuable images.

Hyperspectral microscopy uses Hyperspectral Imaging Spectroscopy (HIS) in conjunction with intricate optics. It constructs characteristic spectral information, similar to that supplied by conventional spectrophotometry, of both infrared and visible light, precisely detecting target materials.

The concept is to fuse the mechanism of spectrophotometry with that of photography. Instead of taking an isolated image at each wavelength for a single pixel, sophisticated algorithms enable the accomplishment of complete spectra per pixel. This provides another layer of information to a typically two-dimensional results.
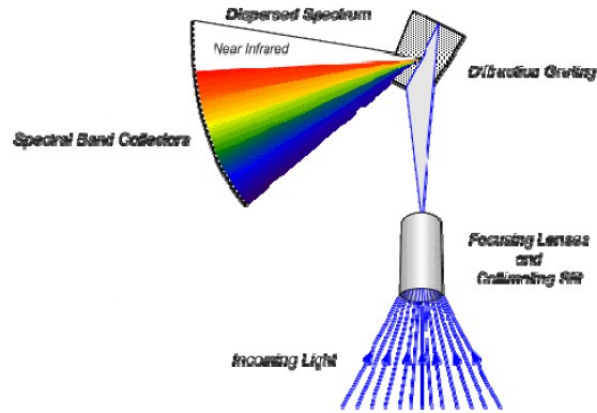
Figure 3.1 Schematic of the diffraction grating of hyperspectral imaging [71].

The dark-field imaging benefits include diminishing the background noise, and underscores the substance that scatters foremost. The CytoViva nano-scale microscope and Hyperspectral Imaging System (HIS) system, as shown in Figure 3.2, which is used in this work, is mounted on an Olympus BX-41 optical microscope. It comprises a dark-field set illuminator that focuses at diagonal inclinations over the sample.
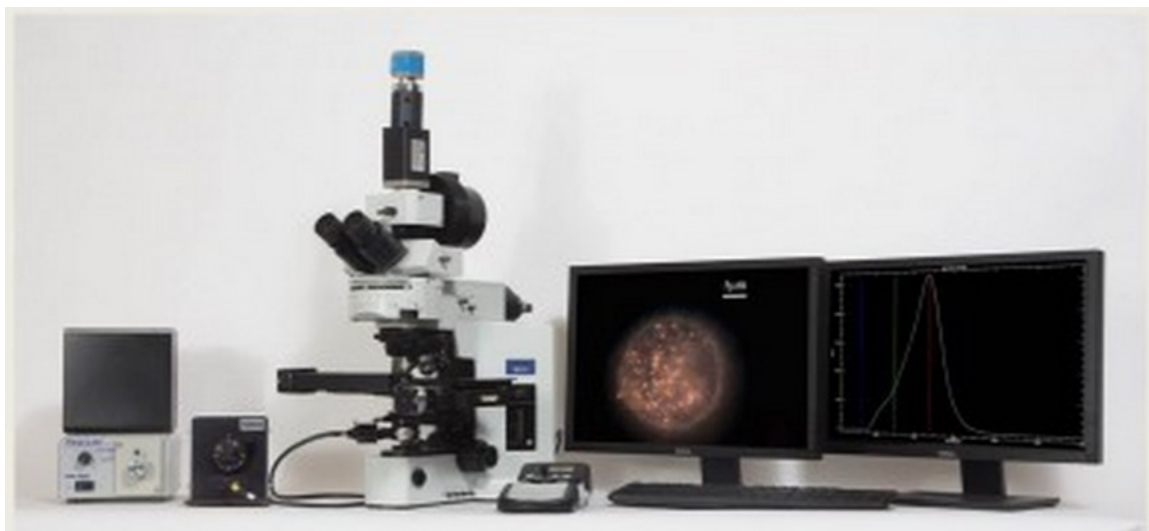
Figure 3.2 Cytoviva nanoscale microscope and HIS system [72].

3.3. Localized Surface Plasmon Resonance (LSPR)

UV-Visible spectroscopy was used to assess the position of the Localized Surface Plasmon Resonance peaks at the varying temperatures.
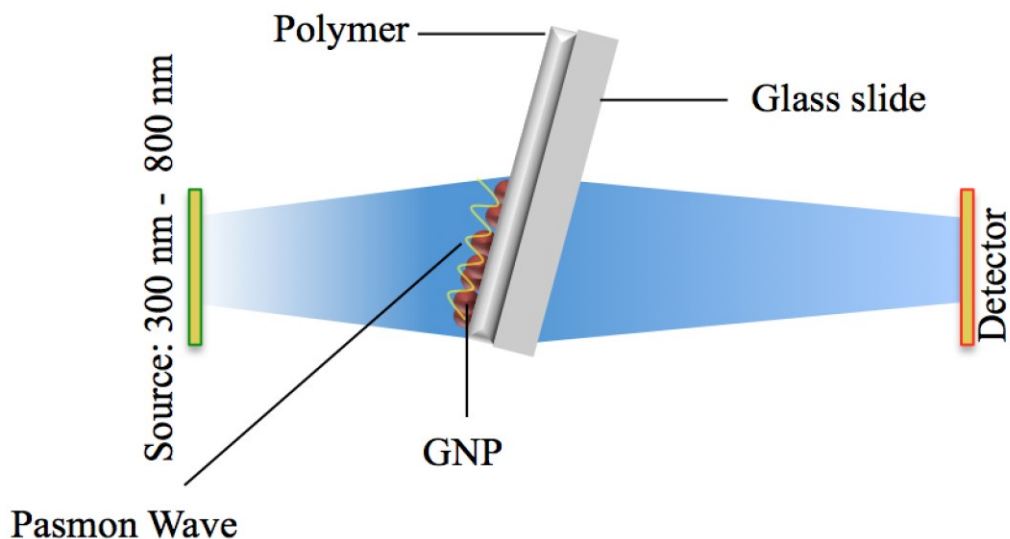
Figure 3.3 Schematic of LSPR measurement with inner workings, including source and detector depicted.

The LSPR spectra depend on the nanoparticles' size, composition and shape, as well as its immediate environment, with plasmons oscillating at the site of the nanoparticle [63]. If a measurement is performed with molecules on a polymer embedded with gold nanoparticles, there runs the chance of the particle being too deep and not being affected by the biological items. If the particle is too deep and the biomolecule is on the surface, there will be no bonding [63].
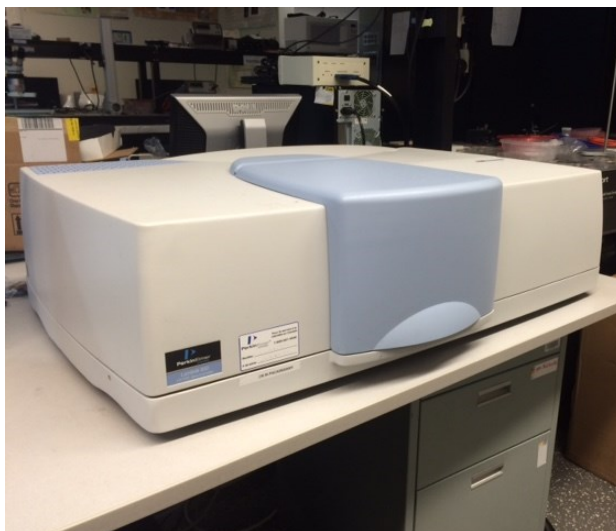
Figure 3.4 The Perkin Elmer: UV/VIS Spectrometer – Lambda 650, used for recording LSPR bands.

3.3.1 Operating Procedure for LSPR Measurement

1. Starting and log in

   1.1. Turn on the machine, the PerkinElmer: UV/VIS Spectrometer - Lambda 650, shown in Figure 3.4, and wait ten minutes for the light to stabilize.

   1.2. Turn on the corresponding software.

2. Properties and zeroing

   2.1. Select data collection and methods settings, and type a wavelength range of 800 nm to 300 nm.

   2.2. Select the number of samples to be measured.

   2.3. Select the auto-zero icon and make sure there are no samples in the machine.

   2.4. Press okay and wait.

3. Sample handling

   3.1. Lift the lid and insert a control slide (clean glass) over the opening on the furthermost support.

   3.2. Handle your samples from the edges, avoiding the area of the gold nanoparticles (purple), and use appropriate holding implements.

3.3. Lean the sample to be measured over the closer support, making certain the light will pass through the intended area (if necessary, use a small plastic layer and prop the slide over it to reach the desired height).

4. Running measurements

4.1. Select the "play" icon and wait for a spectrum to appear.

4.2. Take note of the sample # of the slide and press okay.

4.3. Repeat steps 3.1- 4.2 for the rest of the samples, using the same control slide.

5. Saving and converting spectra

5.1. Save the spectra by selecting "save spectra", then "browse" and locate a suitable folder.

5.2. To convert the files into excel, open the spectrum, click "file," then "export," then "folder," and then pick the same folder.

3.4. Sensitivity Measurements

3.4.1 Operating Procedure Sensitivity Measurements

1. LSPR

1.1. Proceed with LSPR set-up, replacing the control glass slide with an empty quartz cuvette.

2. Cuvette and solvents

2.1. The measured sample will constitute a quartz cuvette with a fragment of the heated GNP-Polymer glass side, as shown in Figure 3.5, and immersed in deionized water.

Glass slide
with GNP
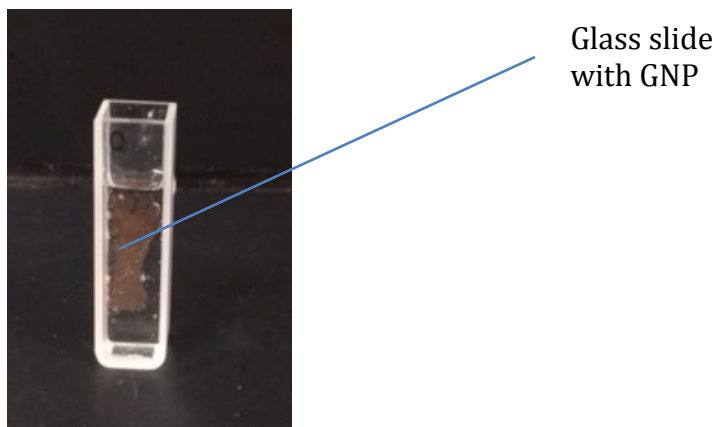
Figure 3.5 Picture of cuvette with edge of gold-polymer composite on glass slide.

3. Replacing solvent

    3.1.   Proceed with LSPR measurements by removing the shard, washing the cuvette and filling it with the next solvent as indicated in Table VI.

TABLE VI. SENSITIVITY SOLVENT AND REFRACTIVE INDICES.

Solvent	Refractive index (n) [62]
Deionized water	1.33
Ethyl alcohol	1.36
2-propanol	1.38
1-pentanol	1.41
N,N-Dimethylformamide	1.43
Toluene	1.50

3.5. Raman Spectroscopy

Raman spectroscopy was utilized to study the gold-polymer interactions. Raman maps were used in order to evaluate possible surface enhancement effects. The parameters that were used are listed in Table VII. The device itself is shown in Figure 3.6. The laser power here refers to the power of the Raman laser that excites the samples, and is related to the intensity of the signal

generated. The largest values that would not damage the sample were used to obtain the most defined result. This device produces very specific spectra by detecting scattered light from the vibrations of molecules in the sample after shining a light source. Another advantage over other spectroscopic techniques is that the spectral bands are narrower and may be isolated and compiled to produce 'map images' that provide a visual representation of a measured area of the sample.

TABLE VII. RAMAN SPECTESCOPY PARAMETERS

Measurement	Range center	Laser power	Laser (nm)
Photoluminescence	2000-3000	5%	514
Raman	1450	1%	785

Figure 3.6 Raman Spectroscopy (Renishaw).

In summary, the techniques used to assess the platform configurations of this work include UV-Visible spectroscopy (Pekin-Elmer's LAMBDA 650), Scanning Electron Microscopy (S-2499n model from HITACHI and Oxford Instruments), Atomic Force Microscopy (3100 AFM model), Raman spectroscopy using a 795nm laser, Fourier Transform Infrared Spectroscopy (FTIR), and Hyperspectral Microscopy (CytoViva). Each gold-polymer nanocomposite platform was assessed with these methods according to compatibility and applicability.

Chapter 4

Simulation

The finite-difference time-domain (FDTD) method makes use of Maxwell's differential equations, which fundamentally define the electric field in relation to the magnetic field spatial changes. In order to produce a distinct electromagnetic field, FDTD employs a second order approximation to x and t derivatives in Maxwell's curl equations. An orthogonal grid of cubes can be arranged in order to calculate the electromagnetic field at systemic intervals of time steps [73].

The FDTD procedure involves computing Maxwell's differential equations by discretization with central difference of time and space. The four Maxwell equations for light are:

$$\Delta \bullet E = \frac{\rho}{\varepsilon_0} \tag{4.1}$$

$$\Delta \bullet E = 0 \tag{4.2}$$

$$\Delta \times E = -\frac{\partial B}{\partial t} \tag{4.3}$$

$$\Delta \times E = \mu_0 J + \mu_0 \varepsilon_0 \frac{\partial E}{\partial t} \tag{4.4}$$

Maxwell's equations connect the differences in time of the electric field E to the differences of space of the magnetic field (H=B/μ), as well as the other way around. The constants μ0 and ε0 are symbols that represent respectively the permeability and permittivity of the medium. J represents the density of the current and ρ is the electric charge density, which is the charge per unit volume. [69]. Throughout the FDTD operations, the material can be defined in terms of properties at each spatial unit [74].

Therefore in this work, a Finite-Difference Time-Domain (FDTD) simulation of the particles

was created to analyze the effects of distribution and depth of particle alterations throughout the heating process. This property was assessed by emulating the localized surface plasmon resonance (LSPR) procedure, as shown in Figure 4.2 [75].

RSoft FullWAVE, a commercial software program for optical applications, was used for the design and testing of the polymer structures, which were approximated as spheres, and defined through the material bank of the program as Au.

This is not the first work with nano-gold items to include such a simulation. In part of his thesis work 'Optical Characterization of Plasmonic Anisotropic Nanostructures by Modeling and Spectroscopic Verification,' Stefan Stoenescu undertook the FDTD simulation of gold nanorods [76]. The fabrication of gold nanorods (AuNRs) involved a synthesis in aqueous solution, where the surfactant cetyl trimethylammonium bromide (CTAB) was added in conjunction with silver nitrate (AgNO$_3$) to enhance axial development. To optimize the optical response, a totally aligned AuNR-PVA composite was used. The resulting spectra of such an arrangement was achieved by performing the FDTD-simulated spectra of a single AuNR, as shown in Figure 4.1, whose 3D representation is also depicted [76].
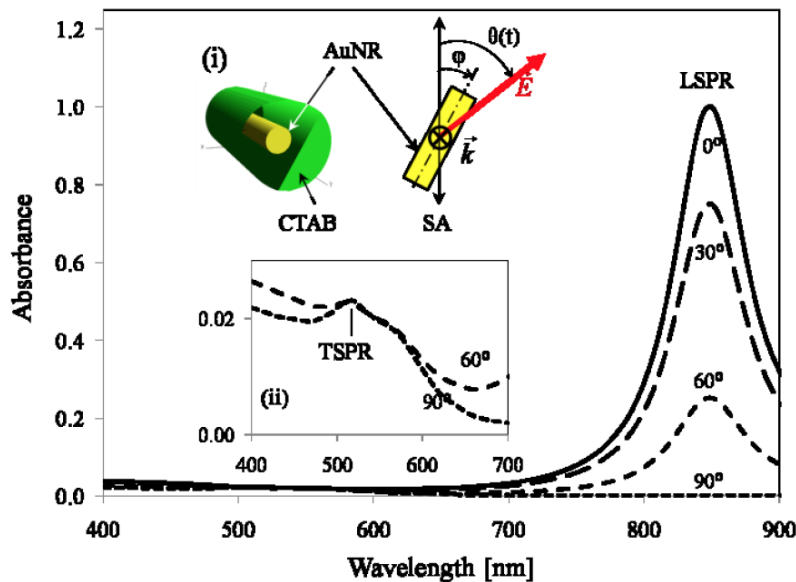
Figure 4.1 Absorbance spectrum of individual AuNR. Inset (i) 3D depiction of NR, coated in surfactant; (ii) absorbance cusp zoom-in [76].

46

Similarly, in his work on nano-islands, Jayan Ozhikandathil [74] performed the finite-difference time-domain simulation and implementation of a morphologically-tuned gold-nano-islands integrated biosensor. In this undertaking, a 3D Finite-Difference Time-Domain (FDTD) simulation of gold nano-islands and nano-clusters was performed. Figure 4.2 (a) has the layout of the simulation, where a gold hemispherical part was targeted by a source with plane waves emanating from a quadrangular launch pad having a transverse electric field.
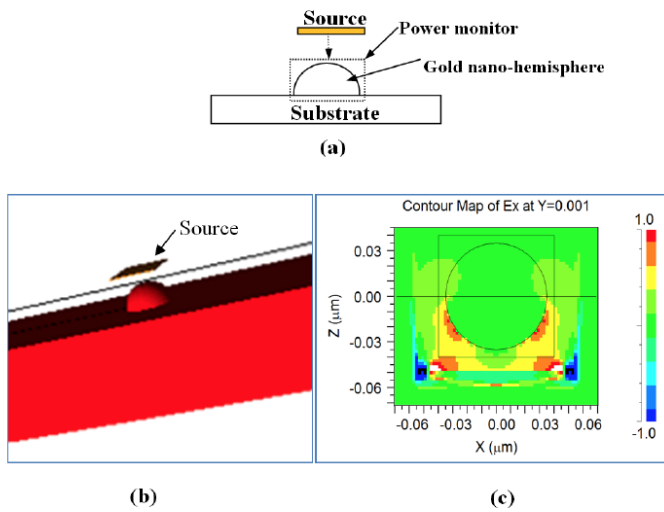
Figure 4.2 (a) the model's configuration; (b) a 3D image of the FDTD simulation; (c) electric field distribution in the gold nan-hemisphere [74].

Another measurement undertaken in this project was examining the FDTD model for the interaction of coupling effects with particles, as shown in Figure 4.3 (a). The arrangement used comprises four gold nano-hemisphere, all separated by distance *d.*
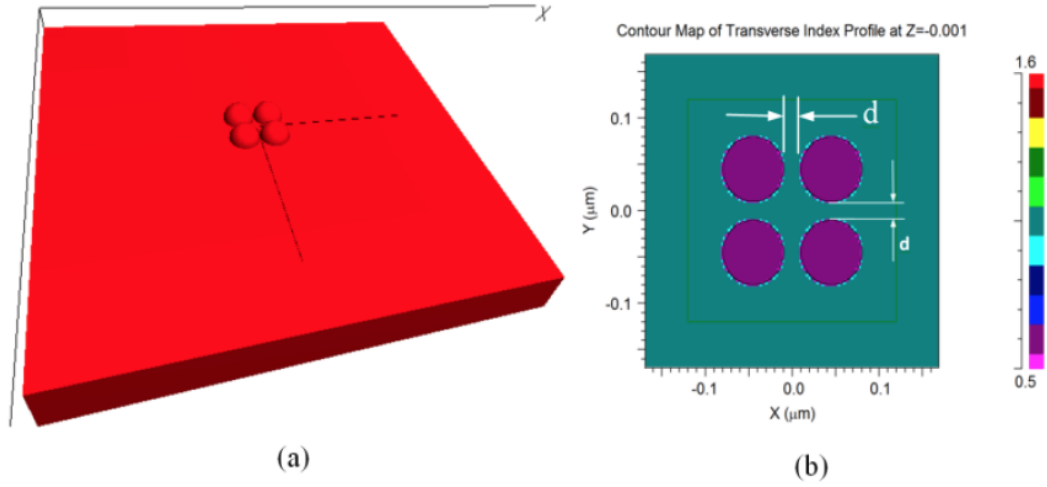
Figure 4.3 (a) FDTD configuration of 4 hemispheres; (b) Refractive index distribution of the model [74].

The effect of the separation distance (*d*) for 4 gold nano-hemispheres on the LSPR property is shown in Figure 4.4.
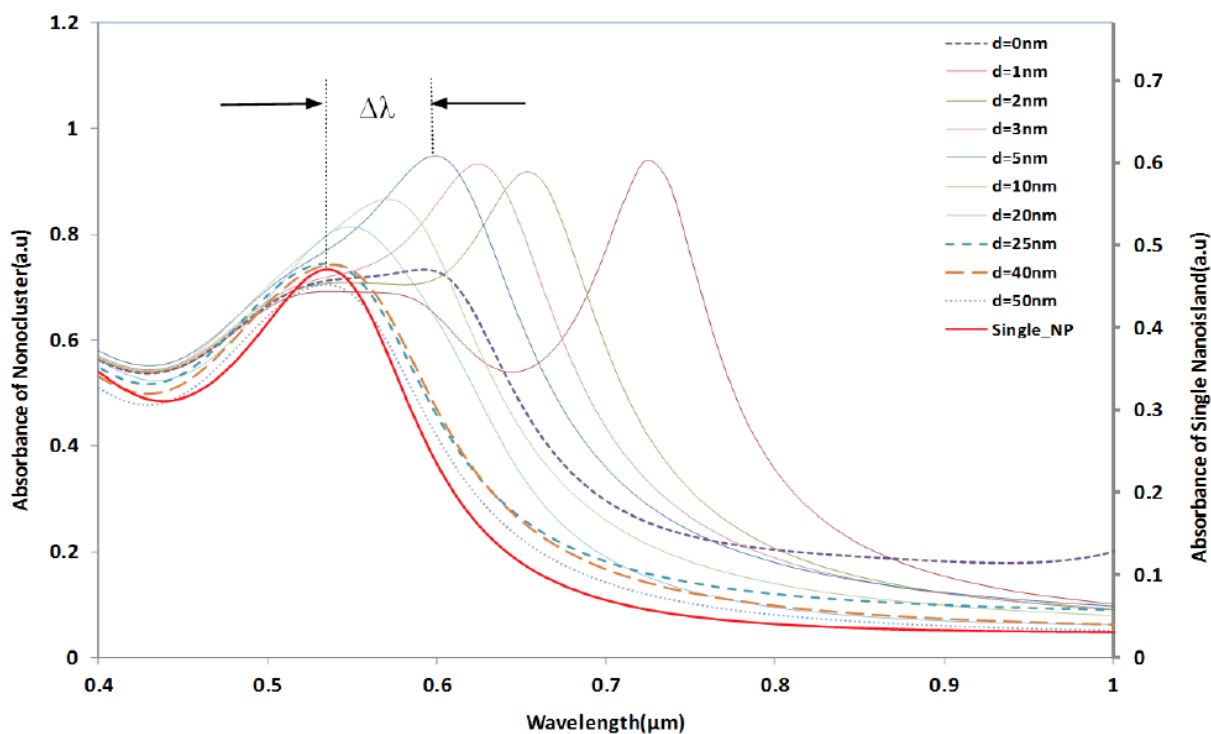
Figure 4.4 LSPR spectra of gold hemisphere when subject to different inter-particle distance 'd' [74].

The resulting patterns indicated that above a distance 'd' of 25 nm, there is little near-field coupling of the hemispheres, and the particle behaves as an isolated feature.

These previous endeavors, though they both involve obtaining the spectrum of gold nano-features, are based on ex-situ arrangements, and do not directly involve gold-polymer composite, a facet in which this project differs [73].

To create the virtual reality of a sphere embedded in a polymer, a merge priority was given to the particles over the films. The technical details of the simulation parameters are as follows: the perfectly matched layer (the boundary condition) is set to 100 nm in every direction, and is placed on the confines of the simulation domain, making the light to be entirely absorbed on the boundary without reflections. In this digital process, the gold nanosphere was excited by a source

49

with plane waves emanating from a rectangular launch pad, having a *transverse* electric field. Additionally, a pulse excitation was selected to impinge the gold nanoparticles.
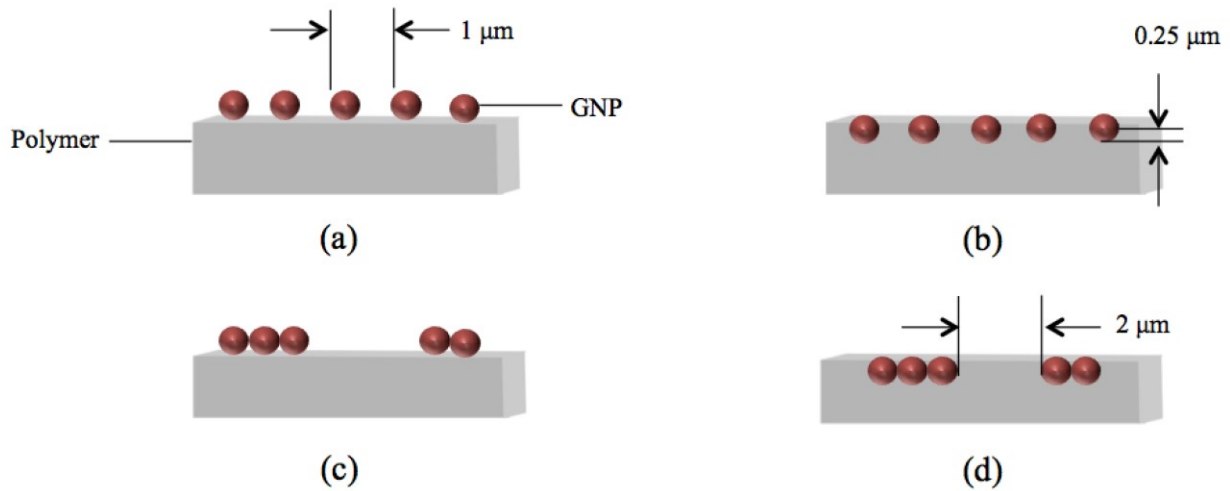

Figure 4.5 Schematic of the four simulated scenarios of gold nanoparticle with polymer, including relevant dimensions: (a) evenly distributed GNP not embedded; (b) evenly distributed GNP embedded; (c) uneven GNP not embedded; (d) uneven GNP embedded.

These were contained in a monitor measuring absorbance from every direction. The electric field distribution on the configuration on the y direction, that is the cross section plane, was simulated by FDTD, and is shown in Figure 4.6. The absorbance spectrum of the gold nanoparticles was calculated through a Fast Fourier Transform (FFT) algorithm. The FDTD method has a precision based on the dimensions of the grid used in allotting the different elements of the equations. The procedure comprises separating the time and spatial field of the task, calculating the relevant differentials, and solving the configuration while accounting for the boundary constraints [72].

In order to generate a simulation of usable precision, the spatial grid must be at least as minute as the smallest aspect of the field to be measured. This value is determined in large part by the material of the simulation.

Since the time domain underpins the FDTD process, FullWAVE has a number of limits that connect to the temporal grid. To produce a steady operation, the Courant condition is important to be respected, as it relates the spatial and temporal step size:

$$c\Delta t < 1/\sqrt{(1/\Delta x^2 + 1/\Delta y^2 + 1/\Delta z^2)} \tag{4.5}$$

where c is the velocity of electromagnetic radiation, and the grid dimensions are derived from the smallest sizes in the simulation. FullWAVE utilizes this property by default [73].

A convergence test is employed to adjust the spatial step after a tentative mesh dimension is selected. This helps reduce any unwanted effects of the mesh size on the electromagnetic response. The procedure involves changing the mesh size, reducing the size until it was apparent that the size no longer affects the results. The chosen size of 1 nm is below the threshold of simulation defects. Another property that had to be picked was the boundary layer. Unless specified otherwise, FullWAVE engages the perfectly matched layer (PML) condition. This consists of a number of points that are located at the ends of the domain. It is intended to behave as a totally lossy border that absorbs the incident energy without generating reflections. PML boundary conditions can be employed in any configuration of the coordinates [73].

Concerning the excitation, the general excitation system consists of spatial and temporal elements, and is composed of an addition of discrete excitations. It can be formulated according to the equations below [69]:

$$\phi_L(\mathbf{r},t) = \Sigma i \, \phi_i(\mathbf{r},t) \tag{4.6}$$
$$\phi_i(\mathbf{r},t) = \sqrt{(P_i)} f_i(\mathbf{r}) g_i(t) e^{i\theta t} \tag{4.7}$$

The arguments of r and t indicate a function of space and time respectively. P_i and ϕ_i are the excitation's power and phase, respectively, and $f_i(\mathbf{r})$ and $g_i(t)$ are the spatial and temporal aspects of the excitation [69].

A pulse excitation, employed in this undertaking, is useful when the frequency response of the model is sought. It uses a Gaussian envelope function multiplied by a sinusoidal carrier, as follows [78]:

$$g(t) = \exp\left[-(t/\tau - t_d)^2\right]\sin[2\pi/\lambda(t) + At^2 + \phi_0] \tag{4.8}$$

where λ is the wavelength, determined by the wavelength field, τ is the pulse time, and t_d is the Delay Time. The factor A, in units of μm^{-2}, allows a chirped excitation. The phase constant Φ_0 is selected in order for the phase to be 0 at the maximum of the Gaussian function [73].

Finally, the frequency generation can be accomplished as a Fourier sum that is derived from a discretized Fourier Transform evaluated over a finite domain. Fast Fourier Transform FFT is the automatic setting for this value. The Fourier sum is as follows [73]:

$$\tilde{\phi}(r', \omega) = \alpha \sum_{t=0}^{t_s} \phi(\mathbf{r}', t) e^{i\omega t}\, dt \tag{4.9}$$

where $\phi(\mathbf{r}', t)$ is the information supplied by the time monitor, t_s is the stop time for the simulation duration, and ω is the frequency.

TABLE VIII. SIMULATION PROPERTIES.

Property	Value/specification
Parts	4
Source	Plane waves/ transverse electric field
Boundary conditions	Perfectly matched layer (100nm)
Particle diameter	0.5 μm
Particle gaps	1-2 μm
Embedding depth	0.25 μm
Particle material	Au (gold)
Interface	'merge' option
Refractive index of polymer	1.5
Detector	Absorbance monitor to replicate LSPR with FFT
Domain grid	10 nm
Particle number	7
Mesh convergence size	1 nm

Four different configurations were tested to examine the different possibilities, as shown in Figure 4.5. The first is a geometry involving nanoparticles, not to scale or relative proportion, over a polymer film, which itself sits on a glass slide. The particles are just peripherally in contact with the polymer. That is, they are not embedded. Additionally, they are perfectly distributed across the polymer surface. The three subsequent iterations follow from this arrangement, varying the dispersion of the particles, and the degree of their sinking
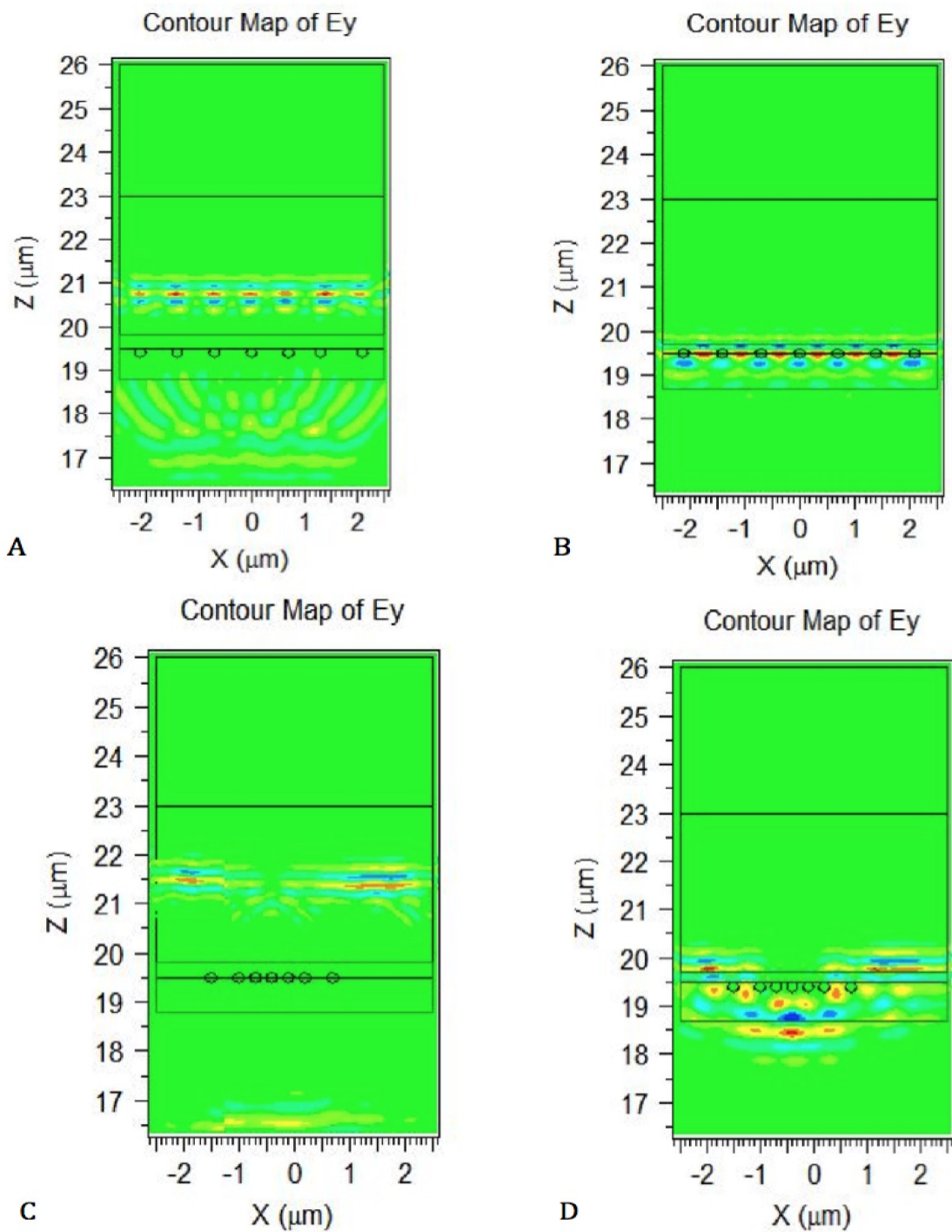
Figure 4.6 FDTD simulations of the LSPR measurements of gold nanoparticles on a polymer: (A) evenly distributed (1 μm) particles not embedded; (B) evenly distributed particles that are embedded; (C) unevenly distributed particles embedded; (D) unevenly distributed particles that are not embedded.

Here, 'Contour Map of Ey' refers to the electric field across the y plane, and X and Z refer to the spatial coordinates of the model. As this is a two-dimensional model, the equation 4.3 describes the linear projection of the electric field, which is related to the varying magnetic field (B) with a time-field distribution across the y plane, the thickness of the slide.

(A)

(B)
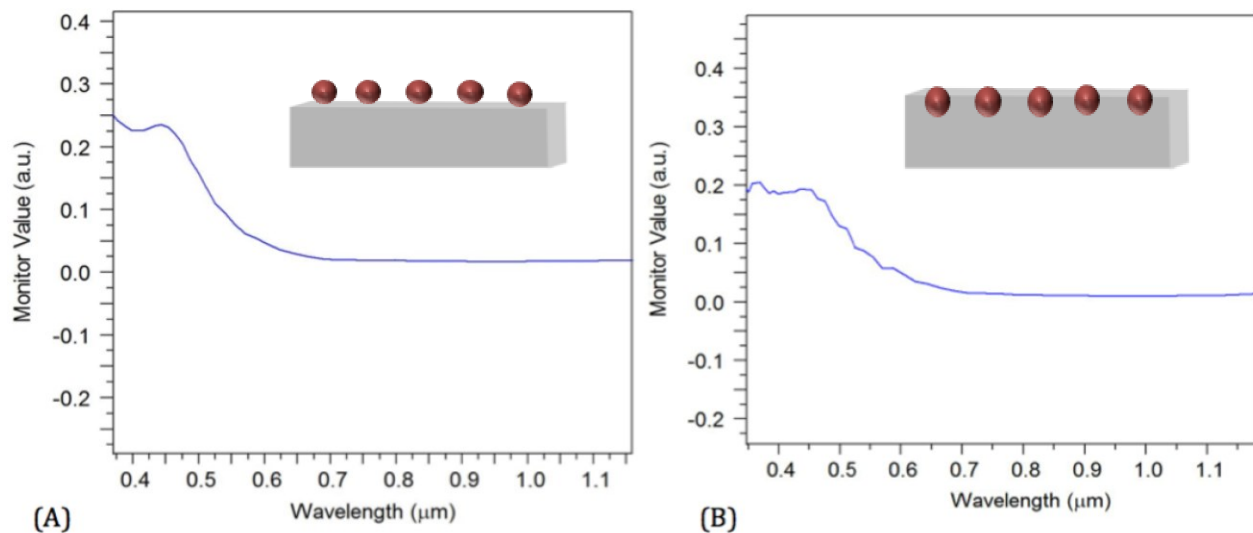
Figure 4.7 The absorption bands of the FDTD tests on evenly distributed GNP: (A) without embedding; (B) with embedding.
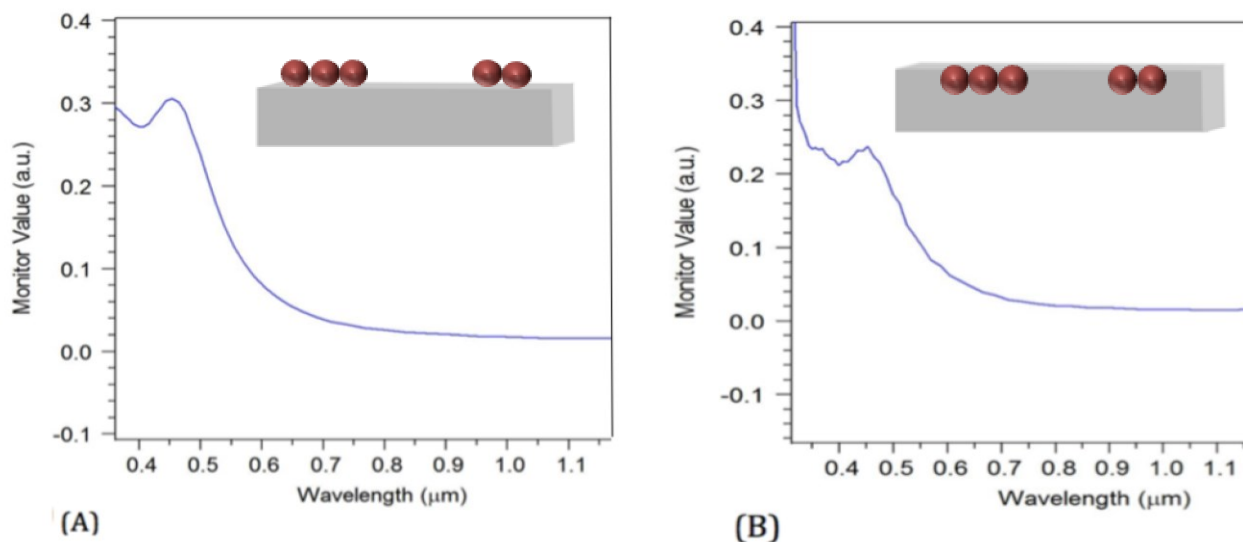
Figure 4.8 The absorption bands of the FDTD tests on unevenly distributed GNP: (A) without embedding; (B) with embedding.

The simulation is made to produce absorbance bands from all four configurations, as shown in Figures 4.7 and 4.8. These are compared to examine the differences in spectra that are caused by particle evenness and embedding. In comparing the first band directly with each other band, it becomes apparent that either a change in distribution or particle depth causes an increase in wavelength of the peak absorbance value. Furthermore, the absorbance peak of 0.22 increases to 0.3 with uneven distribution of particles that are not embedded. The opposite effect, a slight dip in absorbance, occurs when the particles are embedded with even distribution, with a maximum in absorbance of 0.2. The broadness of the curves also is larger for particles that are further apart, indicating that clustered particles yield a sharper peak.

Part of the task in the following chapter, which will be devoted to presenting, analyzing and interpreting the results of microscopic and spectral measurements, is to corroborate the results of this simulation. In particular, the physical LSPR measurements will be helpful in proving the validity of these findings and the trends that were developed from them. However, these results will not be directly contrasted with LSPR graphs, as they are intended to model the trends with heat treatment, and not to derive exact comparisons through juxtapositions.

Chapter 5

Results

The methods that were used to investigate the interaction between the gold nanoparticles and the polymers are: X-Ray Diffraction (XRD), UV-Visible spectroscopy (Pekin-Elmer's LAMBDA 650), Scanning Electron Microscopy (S-2499n model from HITACHI and Oxford Instruments), Atomic Force Microscopy (3100 AFM model), Raman spectroscopy using a 795nm laser, Fourier transform infrared spectroscopy (FTIR), and Hyperspectral Microscopy (CytoViva).

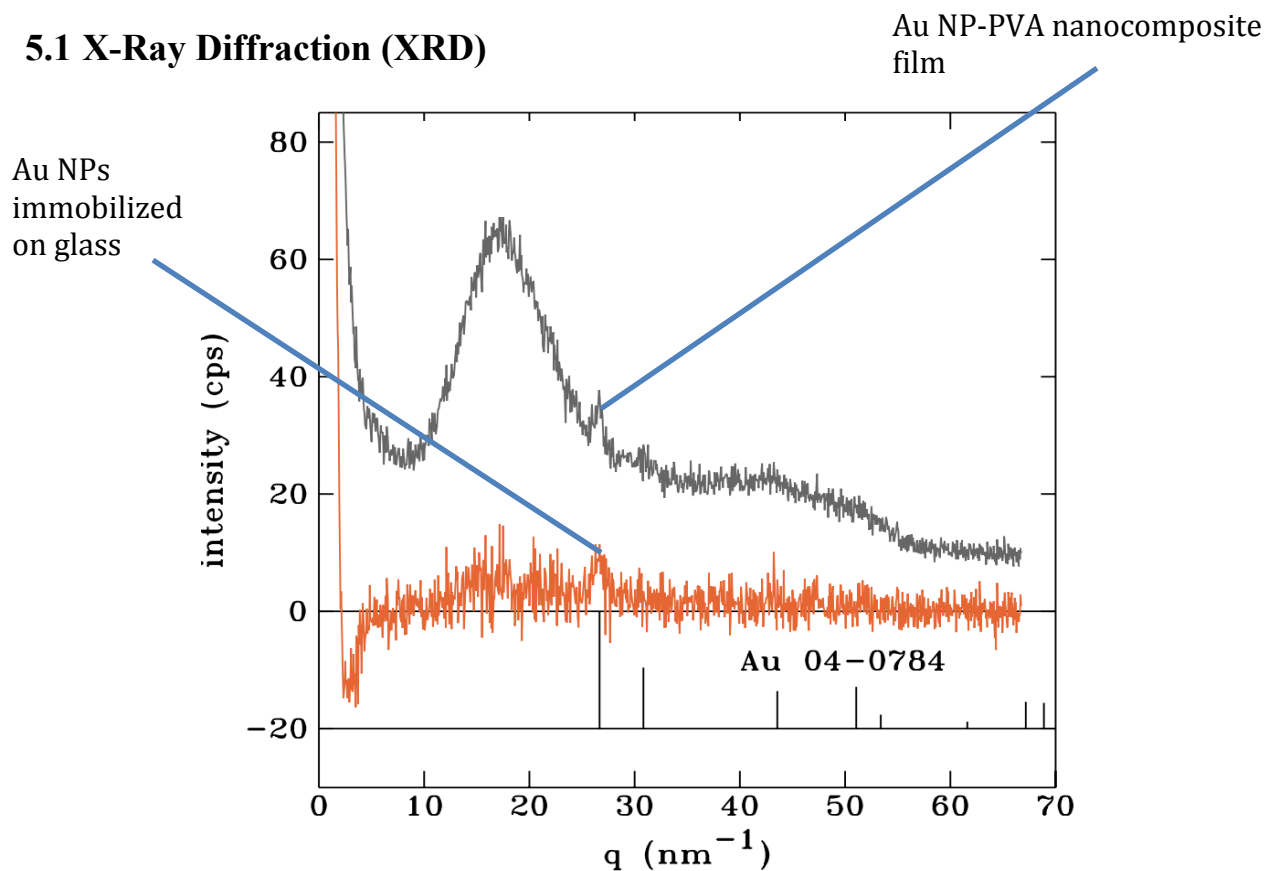## 5.1 X-Ray Diffraction (XRD)

Figure 5.1 X-ray Diffraction (XRD) pattern of: Au NPs on a glass slide (orange) and a PVA sample with Au NPs, heated (black).

X-ray diffraction measurements were performed on a heated PVA substrate with gold nanoparticles, as shown in Figure 5.1, in addition to a glass slide without any polymer with a deposit of Au NPs on its surface. The presence of the polymer results in a strong band at roughly 18/nm, whereas Au NPs and glass alone shows only weak bands. The Au on the polymer substrate appears to be partially crystalline with a small crystal size and broader peaks.

5.2 Scanning Electron Microscopy (SEM)

The images shown in Figure 5.2 reveal the presence of gold aggregates on the surface of non-heated and heated PVA and SU-82 films. The aggregates are distributed over the whole surface of the heated film, as shown in Figure 5.3 (a) and (b). The aggregation of gold nanoparticles has been observed in the case of all polymer films studied in this work that were subjected to repeated cycles of heating and cooling. Generally, the aggregates of gold nanoparticles show a de-clustering tendency when annealed at higher temperatures (around 500 ^{0}C) but in the case of the lower temperatures (200^{0}C) used in this work as well as because of the heating/cooling cycles, the aggregates remain stable. The SEM cross-section images corresponding to Au-PVA and Au-SU-82 nanocomposites are shown in Figure 5.2 to discern the physical interface between gold and polymer. It can be seen that, before the samples are heated (Figure 5.2 (a), the gold particles are evenly arranged across the top of the polymer, and no migration into the polymer is evident. In the images corresponding to the cross-sections of the heated polymers (Figure 5.2(b)-(c)), the gold nanoparticles have migrated (diffused) into the polymer bulk, to various degrees among different polymers. In Figure 5.2(b), which shows the heated PVA sample, it can be seen that a number of particles have undergone penetration across a span of roughly 3 microns into the polymer film. In Figure 5.2 (c), which shows a heatedAu-SU-82 composite, the particles seem mostly gathered towards the top of the sample, but a few nanoparticles can be seen quite deep in the bulk. Similarly, in an experiment carried out by Putla [36], it was observed on a poly(styrene) film bearing Au NPs that the nanoparticles embed into the polymer partially at the end of heating for 10 minutes at 45 °C.
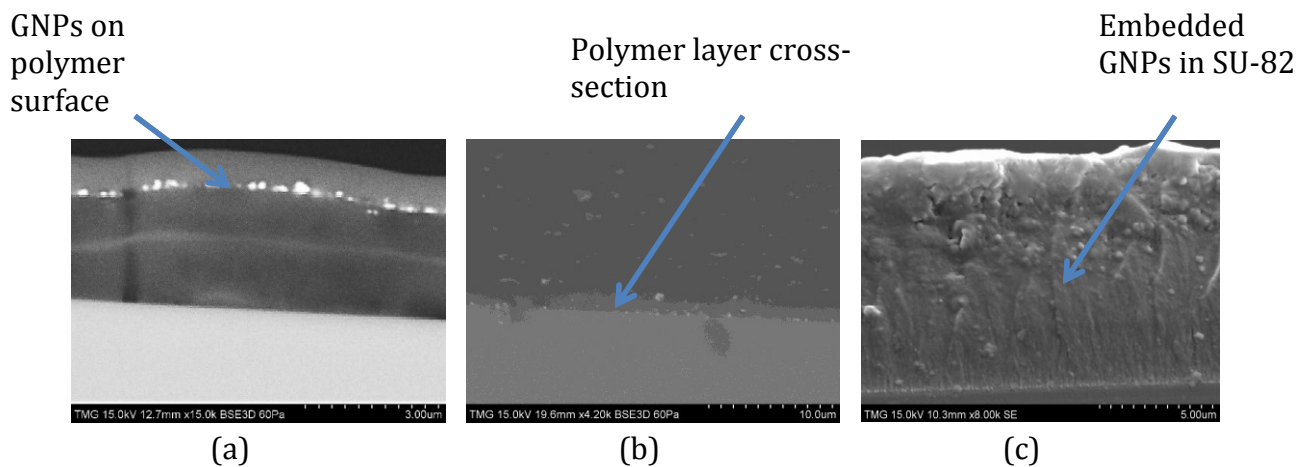
58

GNPs on polymer surface

Polymer layer cross-section

Embedded GNPs in SU-82

TMG 15.0kV 12.7mm x15.0k BSE3D 60Pa   3.00um

TMG 15.0kV 19.6mm x4.20k BSE3D 60Pa   10.0um

TMG 15.0kV 10.3mm x8.00k SE   5.00um

(a)   (b)   (c)

Figure 5.2 SEM images of gold-polymer cross-sections: (a) Au NPs on PVA at 24 °C; (b) Au-PVA nano-composite heated at 175 °C; (c) SU-82 heated at 250 °C.

GNP clusters on heated PVA slide

TMG 15.0kV 6.3mm x1.00k BSE3D 60Pa   50.0um

TMG 15.0kV 5.3mm x19.0k BSE3D 60Pa   3.00um

(a)   (b)
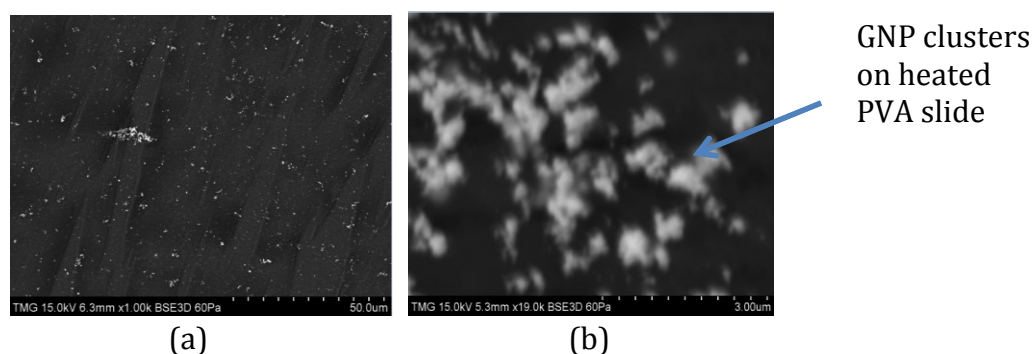
Figure 5.3 SEM images of gold polymer surfaces: (a) and (b) Au NPs on PVA heated at 250 °C.

5.3 Atomic Force Microscopy (AFM)

The surface and cross-section of the Au-PVA nanocomposites were also examined using AFM, as shown in Figure 5.4. The images display an expected discrepancy in surface roughness between heated and non-heated samples. The heated PVA surface, shown in Figure 5.4 (b), has, on average, 20 nm less roughness than a surface of PVA at room temperature, as shown in Figure 5.4 (a). There is also a clear difference in the visual texture of the surface between both images, where the heated sample appears darker in general, with a fewer bright patches. The rightmost image, Figure 5.4 (c), is a cross-sectional view of the heated PVA substrate, showing an aggregation of particles embedded in the bulk of the film. The height indicated, which has a range of 200 nm, may correspond to the horizontal clustering of particles. This is in agreement with the hyperspectral images shown in Figure 5.4.

In related work by Karakouz et al. [77], which involved Au-NPs directly on a glass substrate

without an intervening polymer film, it was found that the morphology of the glass substrate after annealing showed depressions in the glass similar in spacing to the Au NPs.

Lines of roughness

Embedded GNP at cross-section

(a)   **(b)**   **(c)**
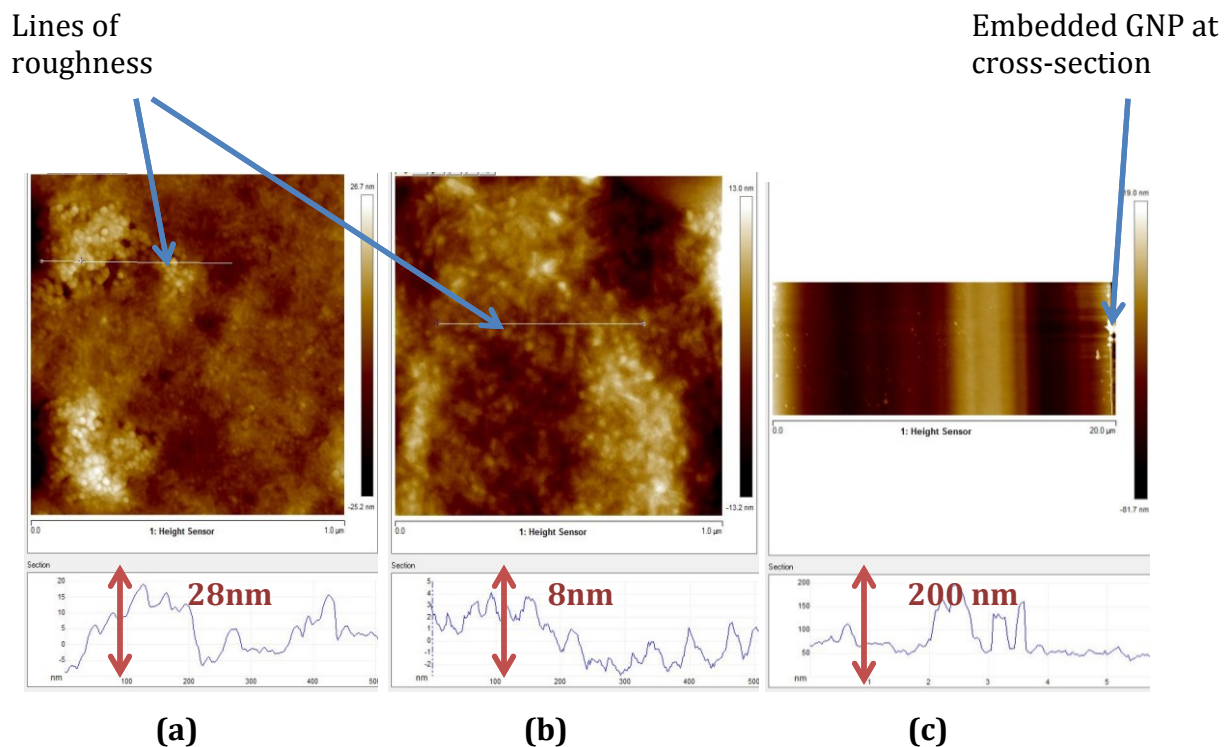
Figure 5.4 AFM image of (a) non-heated Au-PVA composite; (b) AFM image of Au-PVA heated at 225 °C; (c) cross-section of the heated PVA.

5.4 Hyperspectral Imaging

Employing a darkfield hyperspectral microscope, the results of which are shown in Figure 5.6, allows one to detect the substrate with clear and precise images of the particles on the surface of the polymer. Additionally, the spectra analysis may be done at specific regions of interest, enabling the measurement of individual particles and clusters, providing higher sensitivity than LSPR measurements. In Figure 5.5, which shows particles inside a heated PVA polymer layer, the particles seem to have clustered to one area, compared to the image corresponding to the particles in the non-heated polymer. Their LSPR band averages to around 700 nm. In Figure 5.7, which displays the nanoparticles at the surface of the non-heated polymer film, there is a more even distribution and very little aggregation is observed. Individual spectral measurements

average to a lower value (roughly 650 nm) compared with the heated composite. The images corroborate the concept of particle clustering and penetration into the polymer film with heat, and the spectra confirm that when the particles have aggregated, they produce a longer band wavelength as shown also by the UV-Visible spectra of aggregated gold nanoparticles [78].
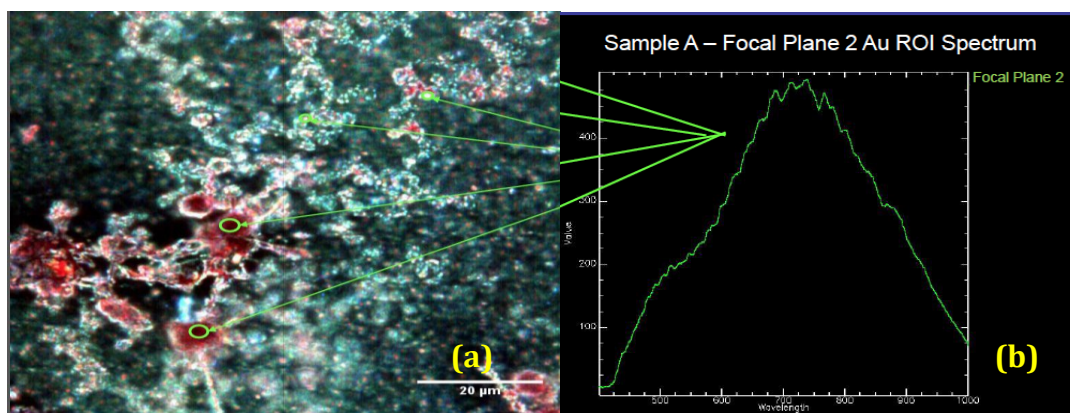
Figure 5.5 Enhanced Darkfield Hyperspectral imaging results of heated PVA: (a) image; (b) spectra.
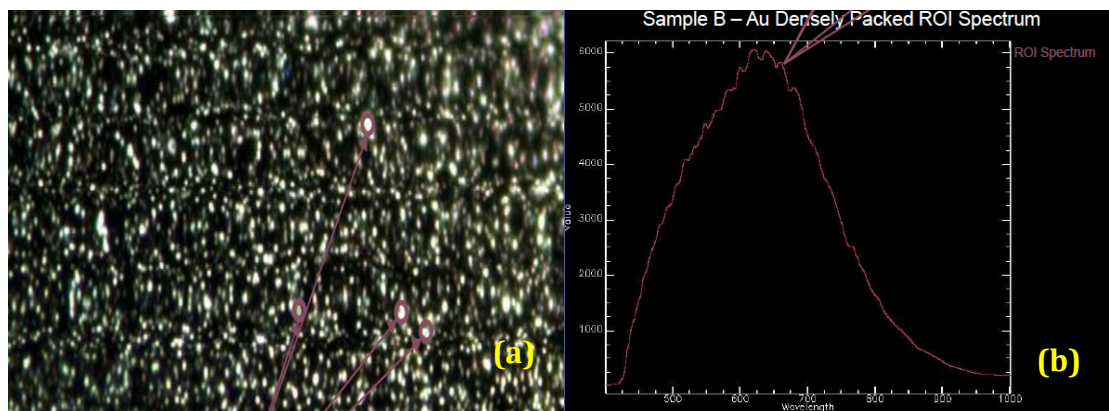
Figure 5.6 Enhanced Darkfield Hyperspectral imaging results of non-heated PVA: (a) image; (b) spectra.

5.5 Localized Surface Plasmon Resonance (LSPR)

Figure 5.7 shows a series of LSPR bands corresponding to six gold nanocomposites with different polymers, throughout the gradation of heat treatments. The graphs display one set of measurements, though three measurements were taken for each temperature increment to

61

confirm the resulting patterns, amounting to 106 useful recordings. These bands correspond to Au-nanoparticles in the surface layer the polymer films. The spectra show that, when the temperature is gradually increased, the bands appear to be shifted to longer wavelengths (red shifts). Karakouz [77] has found that UV-Vis spectra underwent a redshift in the SP band with heating. Similarly, Putla has shown that when the sample temperature is increased to 45 °C in polystyrene, the LSPR band was red-shifted by 4 nm [78].

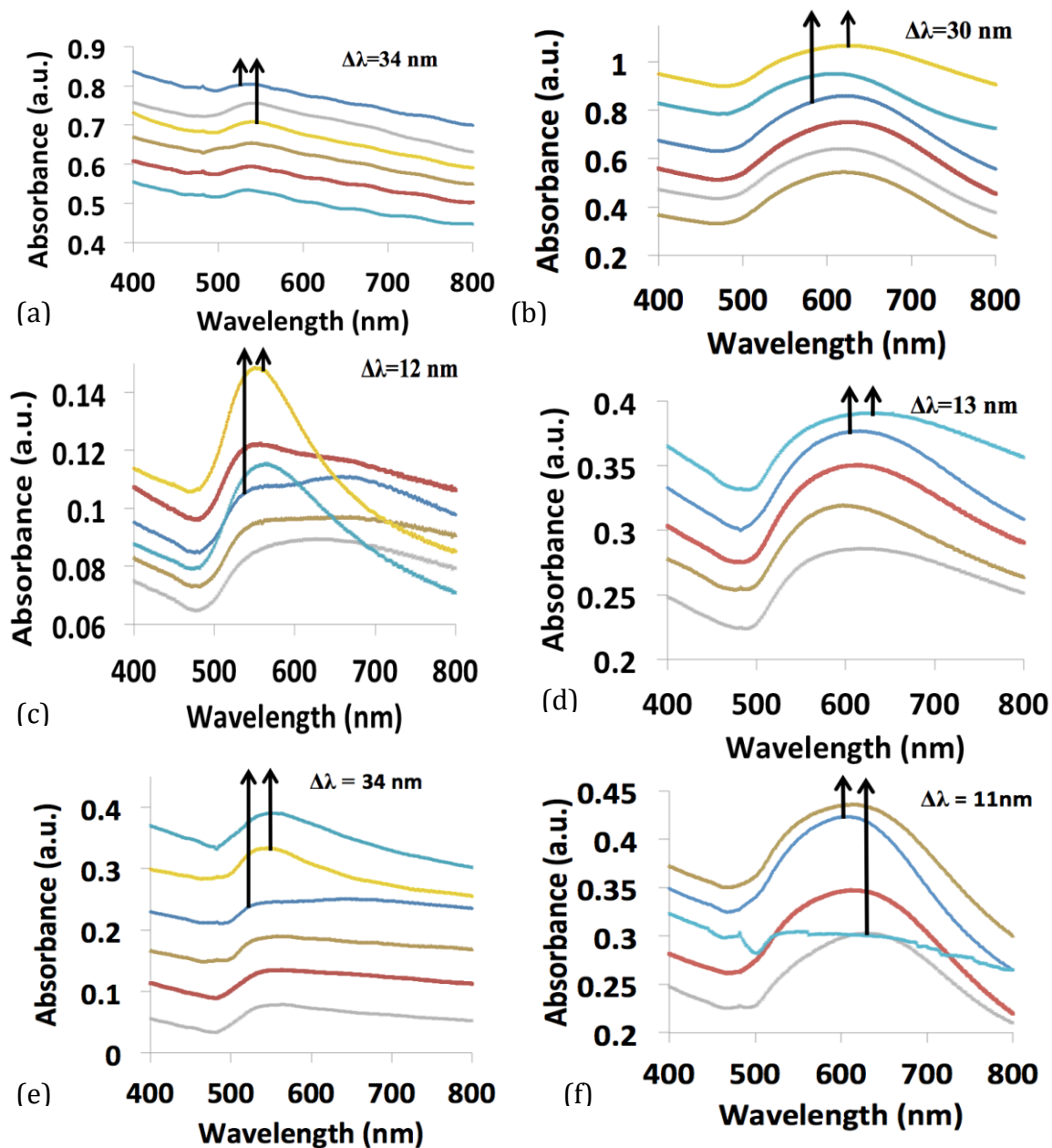**Figure 5.7** Shift of the Au LSPR absorption bands corresponding to selected polymers at different temperatures: 80 °C/dark blue, 100 °C/red, 125 °C/brown, 150 °C/grey, 175 °C/light blue, 200°C/yellow. (a) SU-82; (b) PVA; (c) PDMS; (d) PS; (e) PMMA; (f) COC.
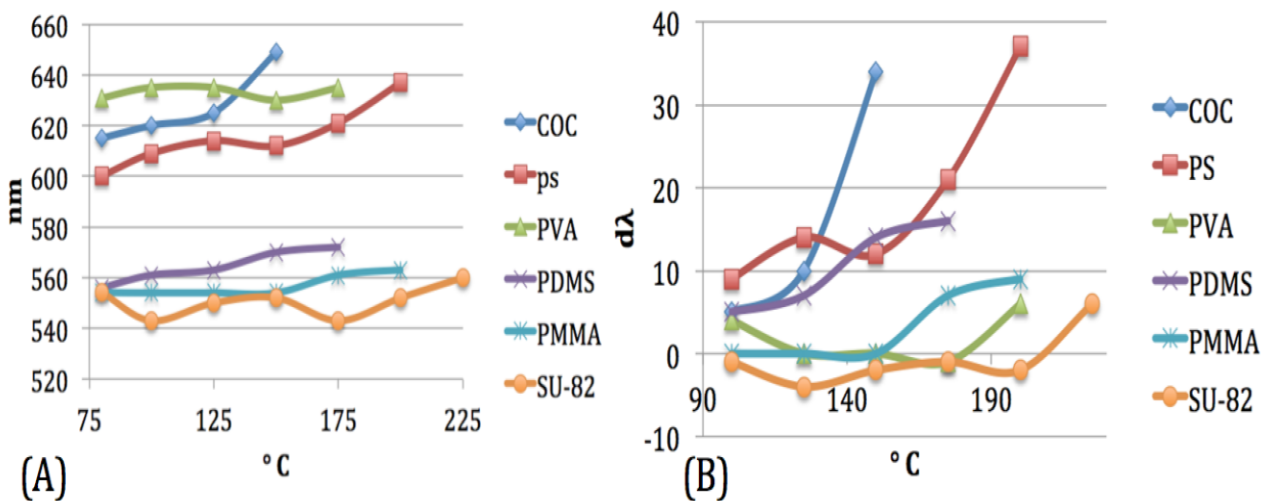
Figure 5.8 Shift of the Au LSPR band for each polymer at corresponding temperatures; (B) Shift of Au LSPR considering the position at 80 °C as a reference.

The Au plasmon band corresponding to Au-SU-82 nanocomposite showed a shift from 525 nm to 559 nm. The transition was mostly steady, with a general pattern of individual bands dipping slighting in the 500 nm region, and then rising again some 50 nm thereafter. The Au Plasmon band of the Au-PDMS nanocomposite shows a shift of 12 nm, rising from the 530 nm value, with the greatest discrepancy occurring at 175 °C. The thermal threshold is defined as the temperature at which the greatest difference between spectral properties is shown. It may indicate the period when the polymer state is most amenable to reconfiguration, and physisorption of gold nanoparticles, which is determined by the surface energy around the particles. An interesting inverse relationship exists between the glass transition temperature values of the polymers and the magnitude of the shift. The polymers PVA and SU-82 show the greatest shifts and a transition temperature (Tg) of 85 °C and 50 °C, respectively, whereas PDMS and PS have Tg of -125 °C and 90 °C, respectively.

Figure 5.9 confirms the higher sensitivity of the Au/PVA nanocomposite, subjected to incremental heating (λ = 627 nm), compared to the sample heated directly to 200^0C (λ = 611

nm). Here as well, three measurements were taken to confirm the pattern. Slides were incrementally heated for all measurements in this work, and the increase in absorbance may be explained by the fact that there is a cooling gradient after the slides are removed from oven. All in all, the incrementally heated slides are therefore subjected to heat for greater durations.
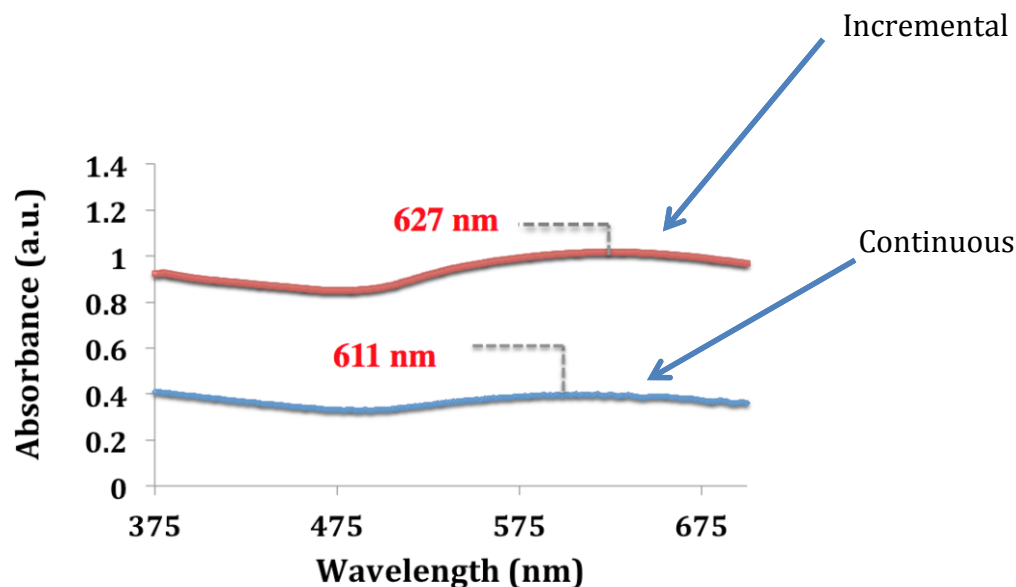
Figure 5.9 Au LSPR band corresponding to incremental-heated Au/PVA sample (red) and to the direct continue heated sample (blue).

5.6 Refractive Index Sensitivity Measurements

The resulting data is incorporated into a graph where the y-axis is the peak wavelength difference to water, and the x-axis is the refractive index difference to water, from solvents shown in Table IX. The slope of the trend-line, measured in nm per refractive index units (nm/RIU), gives an indication of the sensitivity of these gold-bearing polymers. The sensitivity of the nanocomposite platform is shown in Figure 5.10. In correlation with the magnitude of LSPR shifts, PVA and SU-82 display the greatest sensitivity, with 200.64 nm/RIU and 276.74 nm/RIU respectively, whereas PDMS and PMMA have lower values, with nm/123.57 RIU and nm/129.41 respectively. This could be attributed to particles clustering more prominently in some materials, thereby scattering light better, and reacting strongly in response to increasing refractive indices. These results dovetail with those of the LSPR measurements, as the materials

that yielded the greatest wavelengths shifts with heat, such as PVA and SU-82, also had the highest sensitivity values.

TABLE IX. SENSITIVITY SOLVENTS REFRACTIVE DIFFERENCES

Solvent	Refractive index (n) [62]	Refractive Difference (Δn)
Deionized water	1.33	0.00
Ethyl alcohol	1.36	0.03
2-propanol	1.38	0.05
1-pentanol	1.41	0.08
N,N-Dimethylformamide	1.43	0.10
Toluene	1.50	0.17
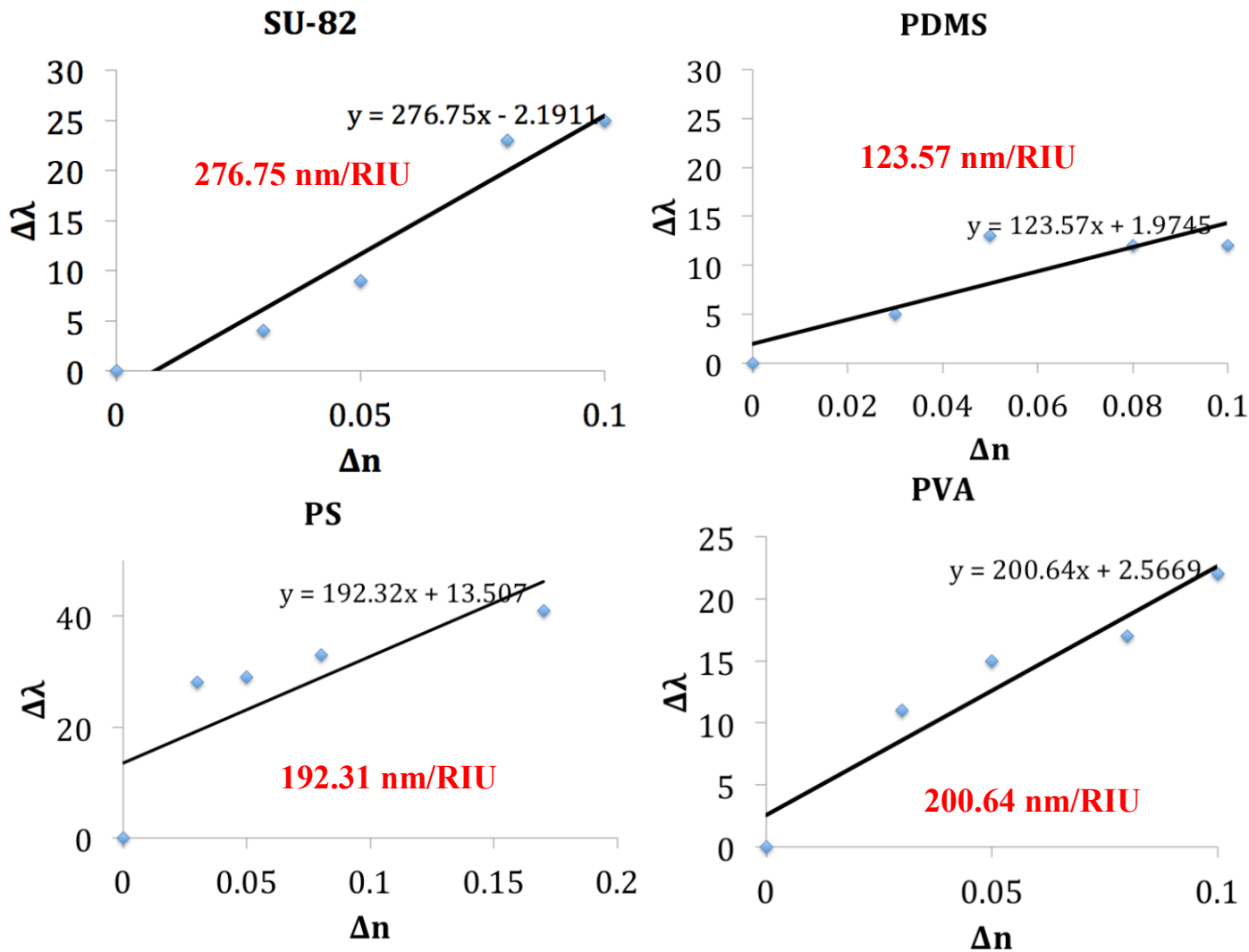
Figure 5.10 Refractive index sensitivity of Au-polymer platforms measuring LSPR shifts in various solvents of different refractive indices.

5.7   Raman Spectroscopy

Figure 5.11 depicts a Raman spectroscopy 'map image' of Au-PVA nanocomposites that is achieved by compiling individual spectral intensities at one band, in this case at 1500/cm Raman shifts. This region is where the polymer exhibits a peak, and the gold material does not. The ratio of the two bands depends on the position of material on the map. A map image was performed for both heated and non-heated Au-PVA samples. In direct juxtaposition, a number of dissimilarities are apparent. There is an even dispersion of red and black (corresponding to gold) patches on the non-heated PVA. In contrast, the heated sample displays a concentration of red

blotches on the top half of the measured area. This trend may result from an aggregation of particles across the surface of the polymer, indicating that, once heated, the polymer is more conducive to particle mobility. Another distinction between the images is the degree of intensity of the spectra. The scale bar at the right-hand of the image of the heated sample is 3289, approximately eightfold smaller than the non-heated sample at 26284. This may be due to a smoothening of the polymer surface as result of the embedded gold nanoparticles in the polymer, which would diminish the protrusion of particles across the polymer surface and decrease spectra intensities. Karakouz et al. [77] has found that, with polystyrene, annealing for 10 h at 600 °C leads to aggregation of closely spaced NPs, forming considerable clusters of particles.
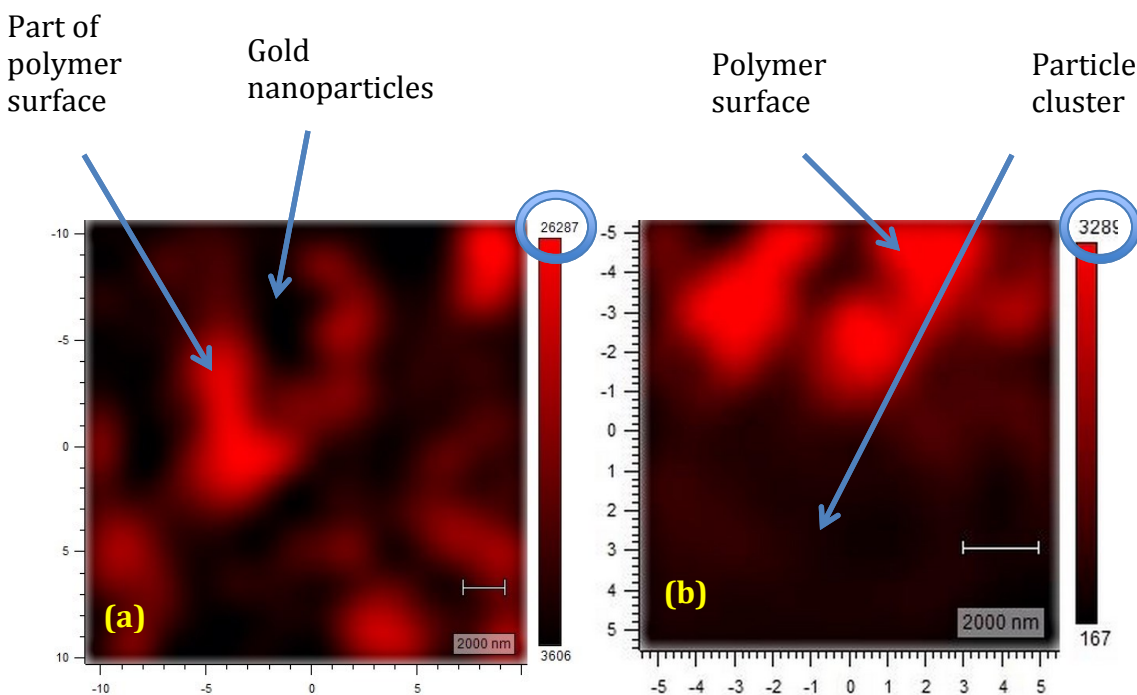

Figure 5.11 Raman Spectroscopy Map (image created from compilation of seperate Raman spectra) for a) non-heated Au-PVA (10 μm x 10 μm); (b) and heated at 175 °C (20 μm x 20 μm).

The corresponding spectra of the Raman measurements taken at roughly 1400 Raman Shift, as shown in Figure 5.12 and 5,13, indicate the ratio of the two bands depends on the position of material on the map.
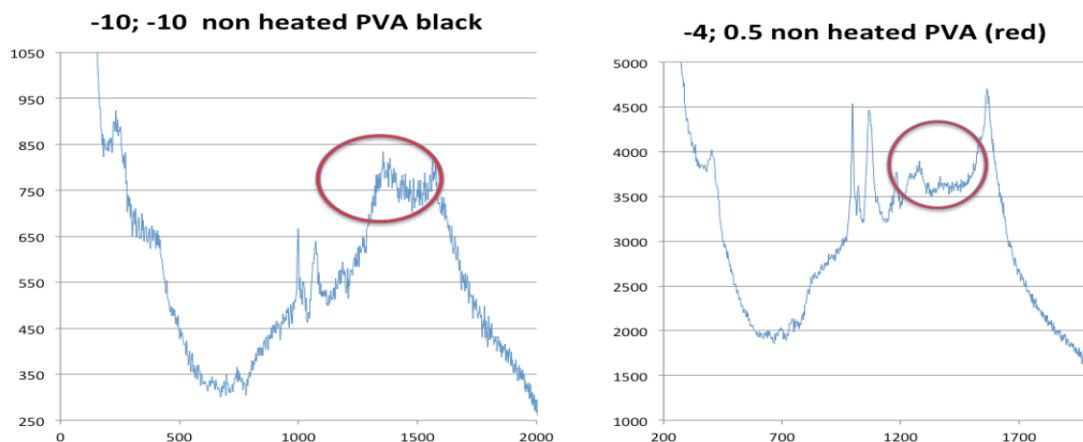
Figure 5.12 Raman Spectra of black and red areas from the map image of a non-heated sample.
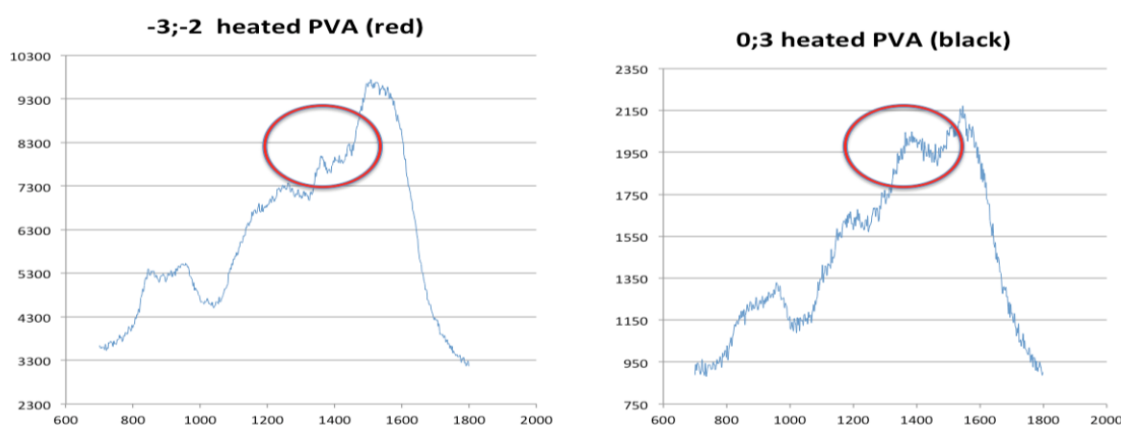
Figure 5.13 Raman Spectra of black and red areas from the map image of a heated sample.

5.8 Fourier transform Infrared Spectroscopy (FTIR)

Another measurement made was that of Fourier Transform Infrared Spectroscopy (FTIR). As glass is a poor transmitter of infrared wavelengths, the only sample measured in this fashion was COC, as here the material was bought as a film, and did not require spin coating over a glass slide. The resulting spectra, shown in Figure 5.14, corroborate the findings aforementioned. Namely, heating a polymer bearing gold nanoparticles on the surface will result in part in the sinking of particles. This can be inferred from the resemblance of the spectra of the heated sample with gold and the sample without gold, both comprising sizable peak at roughly 3000

wavenumbers (cm^{-1}). This value is not as apparent in the spectra of Au-COC composite without the heat. It is feasible the particles not only embedded into the polymer layer, but also clustered into deeper groups, further diminishing the polymer band.

Figure 5.14 FTIR spectra of: (a) COC sample not heated with GNP; (b) COC sample heated with GNP; (c) COC sample not heated without any gold.

In summary, both the morphological and the spectral studies are showing marked differences between the Au – polymer nanocomposites studied in this work. The differences originate in the structure of the surface layer of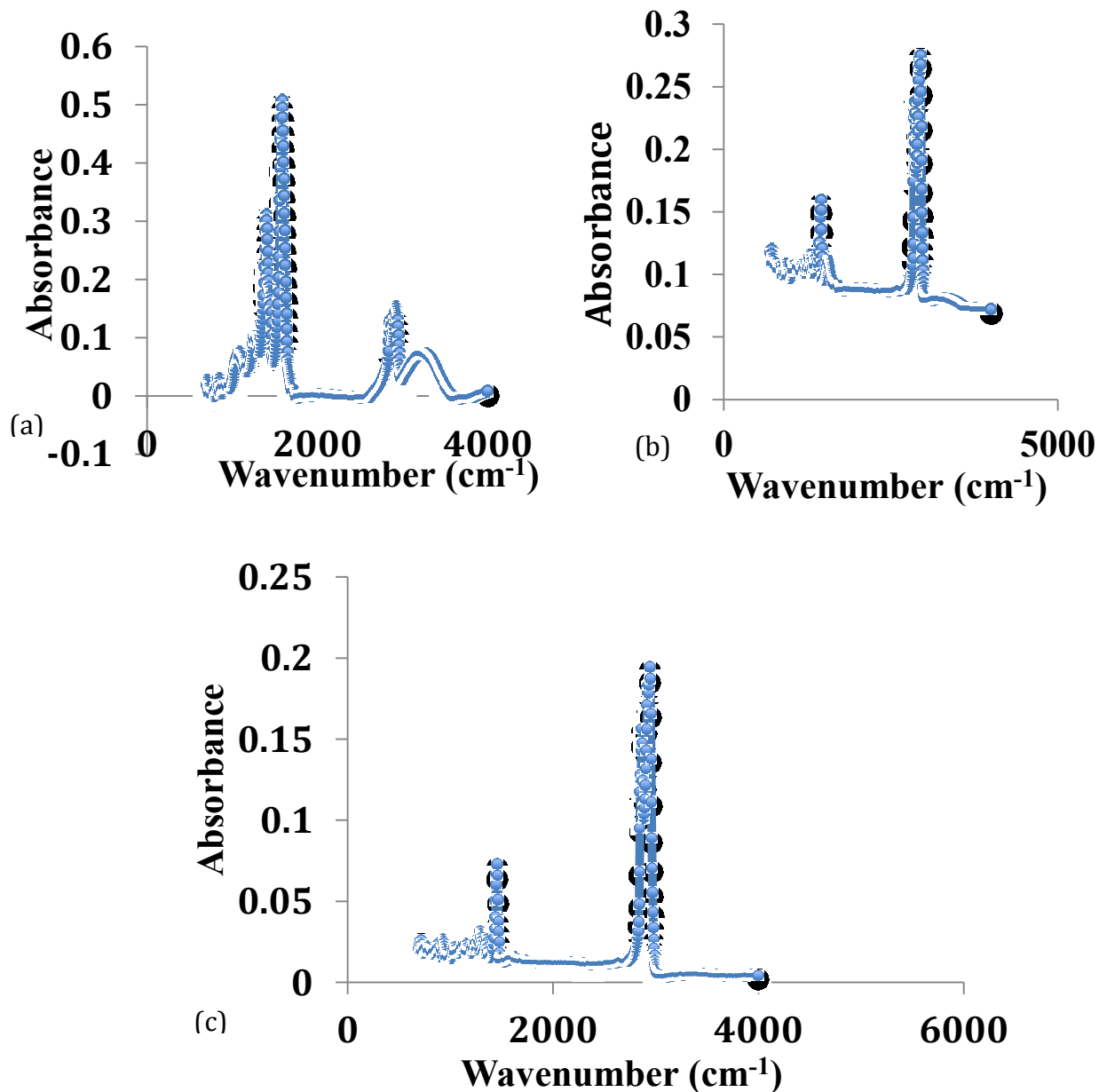 the polymer where the gold nanoparticles are hosted as well as in the specific thermal properties of the polymer, that is, their softening and glass transition temperatures, respectively. The position of the Au LSPR band in the nano-composite, which is extremely sensitive to the dielectric environment, is the result of several concurrent phenomena, namely, softening of the polymer surface layer and partial or total embedding of gold nanoparticles, formation of gold aggregates having various sizes and shapes, and, possible interactions between the gold particles or aggregates and the polymer chains. From this point of view, one can understand why the Au-PVA nanocomposite band shows an enhanced sensitivity after the heat treatment. Indeed, the polymer has a bulk glass transition temperature of $85^{0}C$, the AFM and SEM images shows some embedded particles into the surface layer and the presence of gold aggregates on the surface.

5.9 Protein Biocompatibility

The methods utilized to assess the interaction between the green fluorescent protein (GFP) and the polymers are: fluorescence microscopy (20X with a green filter), atomic force microscopy (3100 AFM model), plasmonic spectroscopy (PekinElmer's LAMBDA 650), fluorescence spectroscopy, as shown in Figure 5.15, and scanning electron microscopy (S-3499n model from HITACHI and Oxford Instruments).
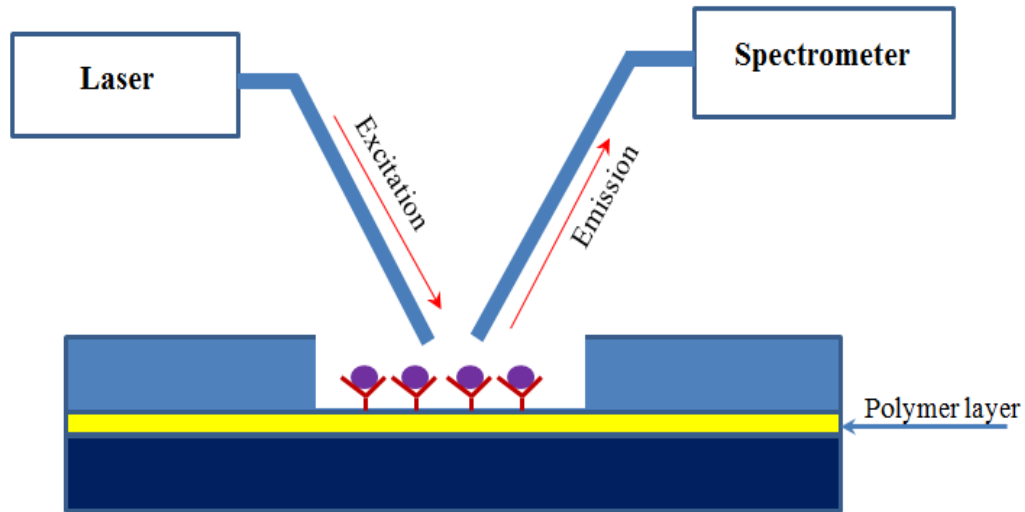
Figure 5.15 Experimental setup for measuring the fluorescence emission of GFP on the polymer substrate.

The microscope was used to assess the amount of antibodies attached to the various polymer films by leaving the protein solution on them for 24 hours, and then washing them with PBS. A green filter was employed in the endeavor to excite the fluorophores (excitation wavelength of 395 nm). The light intensity was adjusted according to the haziness of the image, which differed from one polymer to the next.

5.9.1 Procedure for Protein Preparation

1. Preparation
   1.1. Prepare 50 ml of phosphate buffered saline (PBS) in a volumetric flask by transfer with a syringe and funnel.
2. Solution
   2.1. Dump two bottles of antibody of mouse anti-GFP (100 µg) into flask.
   2.2. Wash funnel and place the syringe with the volumetric flask in a beaker and refrigerate.
3. Linker
   3.1. Apply linker (1-octadecanethio NanoThinks 18) in droplets to glass slide deposited with GNP using a micropipettes in droplets.

3.2. Leave the samples in the fume hood to dry for a day.

4. Antibody

4.1. Apply the antibody (Mouse Anti-GFP – Invitrogen) to the slide through droplets by micropipettes to spread evenly across region of interest (approximately 50 µL).

4.2. Take measurements immediately with spectroscope or wait to dry and take note of the state of the solution (crystallized or liquid).

5. Antigen

5.1. Add the conjugate antigen (GFP, AEGUOREA Protein, Recombinant N-His tag Invitrogen) in the same fashion and take measurements.

5.2. Reverse steps 6 and 8 for alternate measurements.

A Scanning Electron Microscope was used to study the morphology of gold nanoparticles adsorbed on the polymer films. For the fluorescence spectroscopy measurements, the protein solution was deposited on the polymer substrates and a 395 nm ultraviolet light-emitting diode, which was illuminated using 3.0 volts, was shining directly on it, under a photo-detector, which transmitted the signal to an Ocean Optics software. The excitation wavelength is 395 nm and the emission wavelength is 508 nm for the fluorophores.

Figure 5.16 shows the microscopic images of the polymers slides after bearing a deposit of GFP for 24 hours before washing, with PMMA (Figure 5.16(a)), PDMS (Figure 5.16(b)), PS (Figure 5.16(c)), and COC(Figure 5.16(d)).
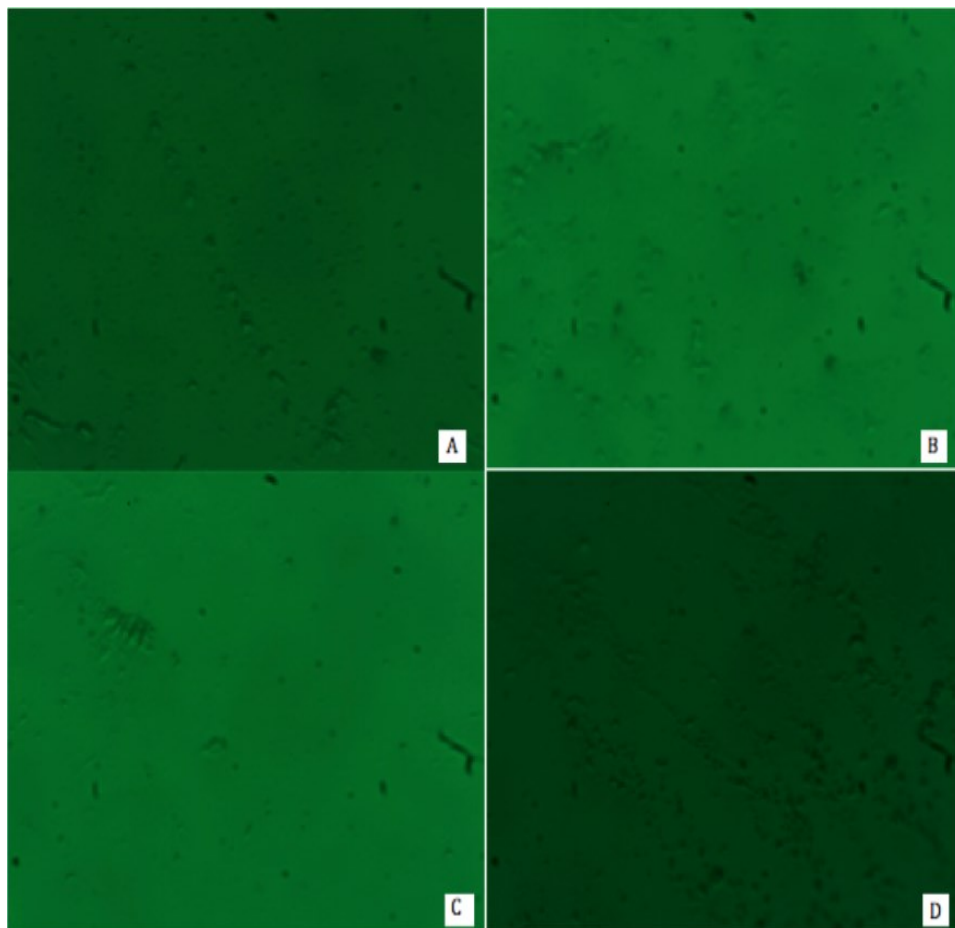
Figure 5.16 Microscope images of (a) PMMA, (b) PDMS; (c) PS; (d) COC with protein attached to the polymer after washing.

The GFP adsorbed onto the substrates was also investigated using AFM characterization, as shown in Figure 5.17. The images show an important amount of GFP attached to the PVA and PMMA surfaces (hydrophilic polymers) and significantly less to SU82 and PDMS (hydrophobic surfaces). Protein aggregates can be seen on the PDMS surface.
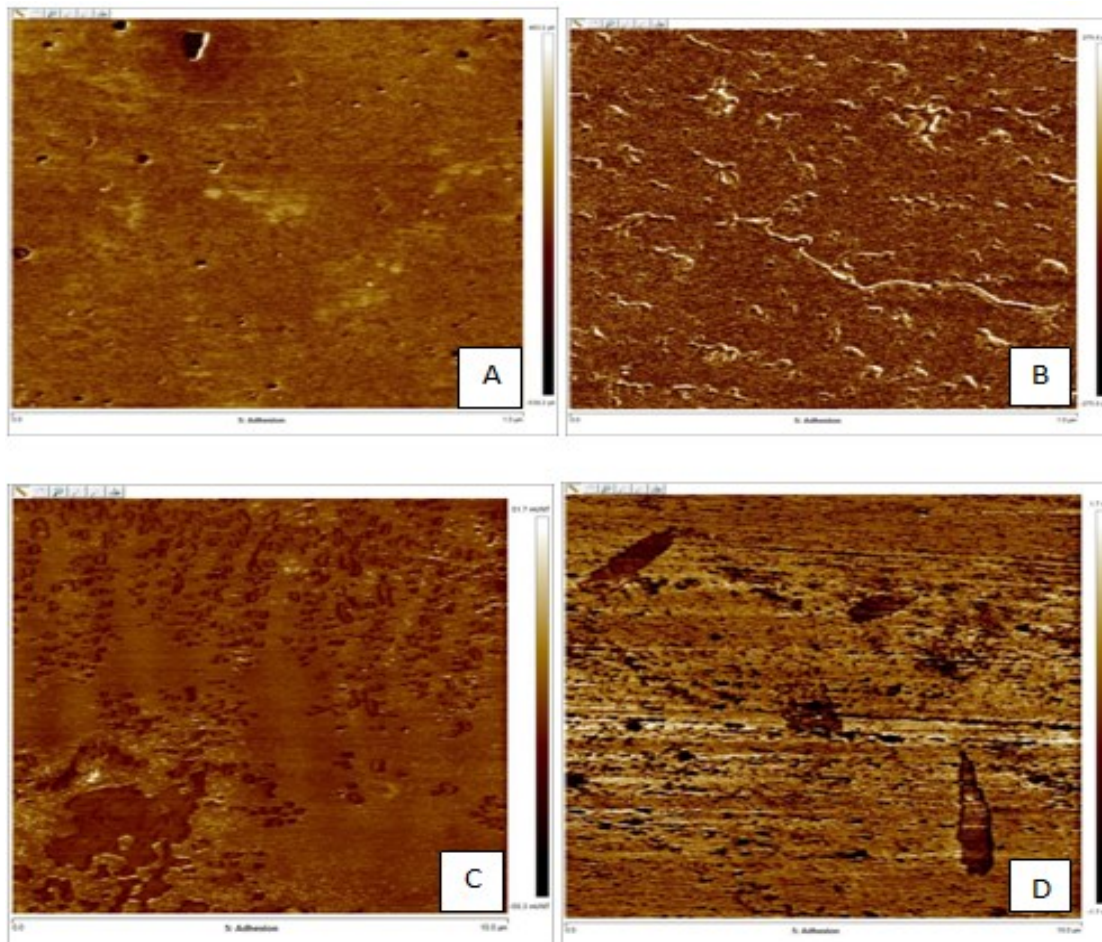
Figure 5.17 AFM images of the polymer surface with the attached GFP. A) SU-82 B) PMMA C) PVA D) PDMS.

Figure 5.18 depicts the SEM images of various polymers with gold nanoparticle deposits. PMMA and PVA appear to have higher concentrations of particles, B and D respectively, as opposed to SU-82 and PS, A and C respectively. This result corroborates with the GFP affinity as found from the AFM images. The size of the particles, as is annotated in the illustrations, ranges from 66 nm to 427 nm, with the majority being approximately 100 nm in diameter. Additionally, polymers SU-82 and PS have, in general, smaller particles less densely packed, in contrast to PMMA and PVA, which appear to have particles of greater dimensions and concentrations.
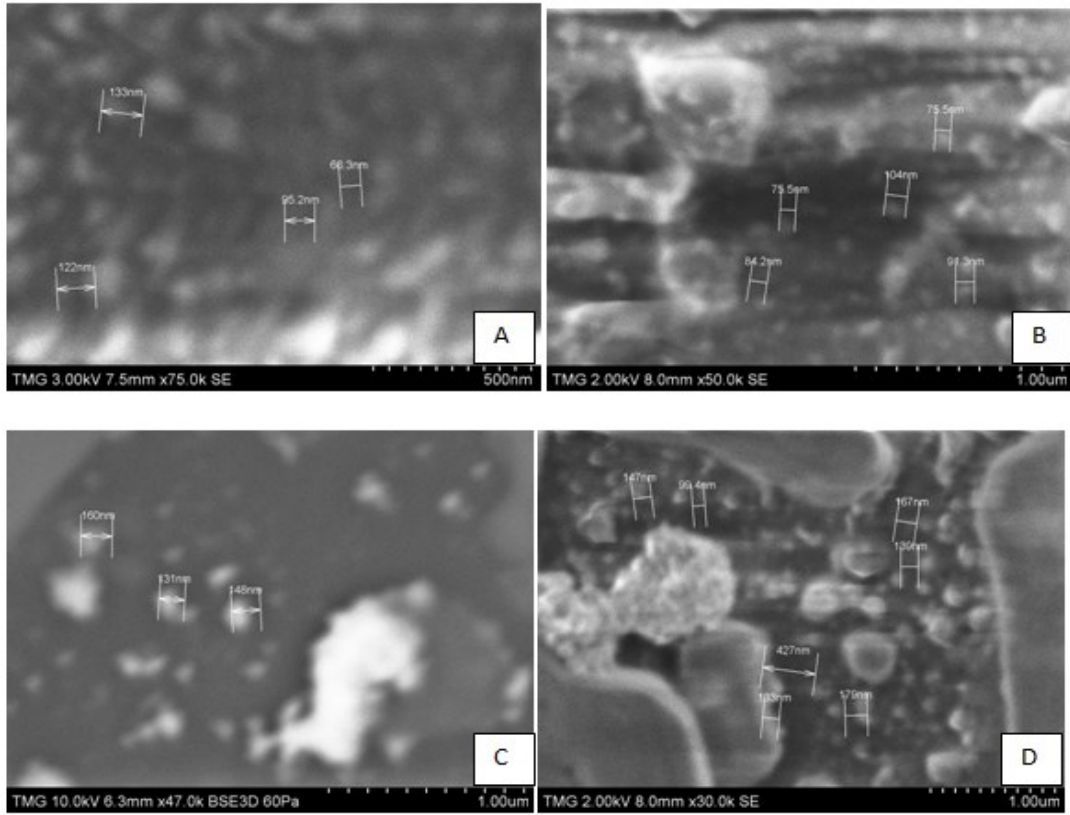
Figure 5.18 SEM images of SU-82 (A); PMMA (B); PS (C); PVA (D).
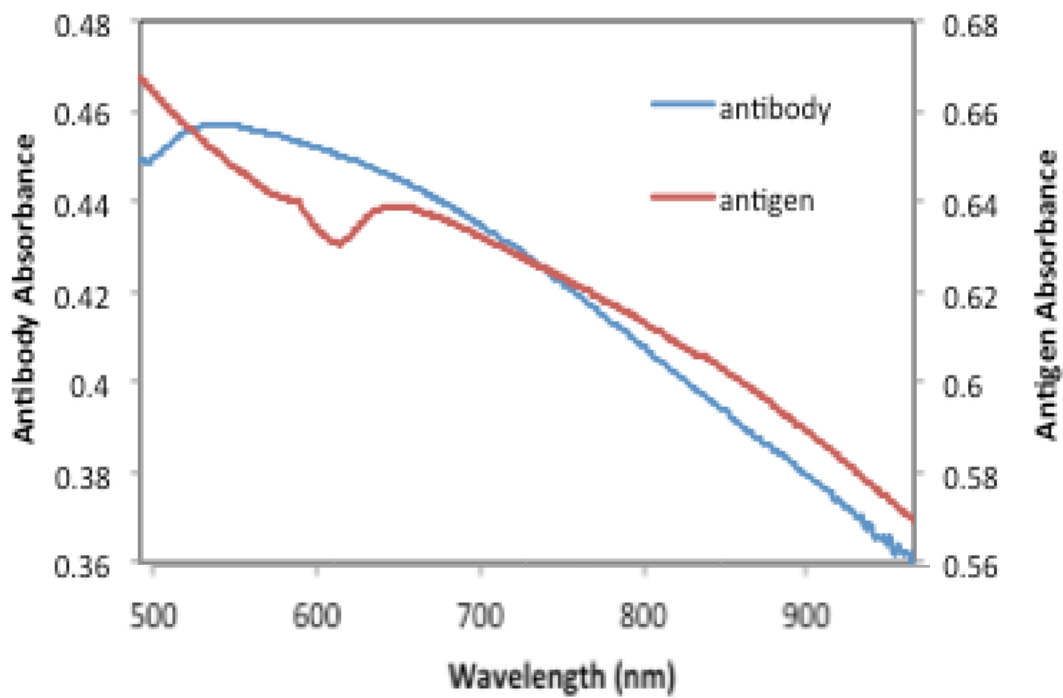
Figure 5.19 Shift (Δλ) of the Au LSPR band due to Ab-Ag interaction (Ab: Green fluorescent protein monoclonal antibody; Ag : Green fluorescent protein).
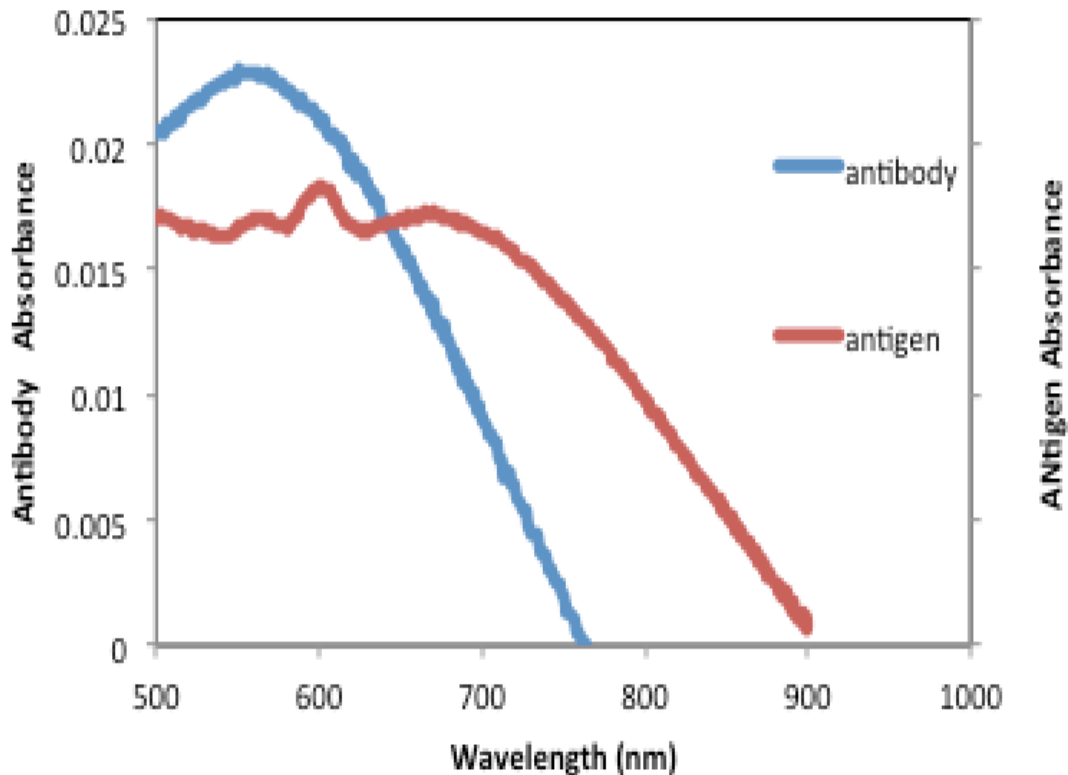
Figure 5.20 Shift of Au LSPR band due to the Ab-Ag interaction (Ab: Green fluorescent protein monoclonal antibody; Ag : Green fluorescent protein).

As a comparative standard value, each polymer was illuminated without the protein solution, which produced nearly identical patterns of no alterations in emissions, as shown in Figure 5.20. The result has shown a high intensity of the fluorescence emission corresponding to PS, COC, and PVA, and a lower for SU82, confirming the higher affinity of GFP to polymers with hydrophilic surfaces.
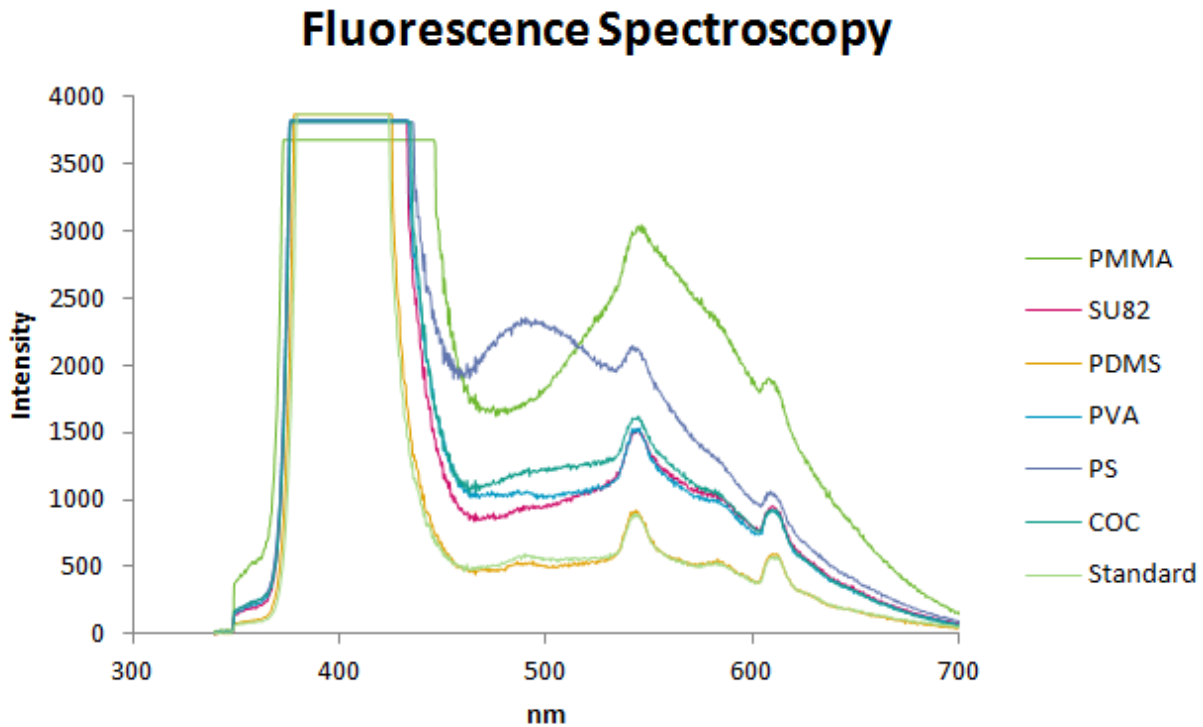
Figure 5.20 Fluorescence spectra of polymers in contact with droplets of GFP.

In summary, all the methods used in this work, whether to assess cross-sectional or surface areas of the gold-polymer nanocomposite platforms, or protein affinity and polymer sensitivity, uniformly indicate that gold nanoparticles sink into the underlying polymer layer with systematic heat treatment and, simultaneously with this, form aggregations. In general, more heat leads to more particle penetration, making the obtained data useful for balancing the desire to drive-in the GNP without completely engulfing them in the polymer material. Furthermore, PVA and SU-82 are the materials that showed the greatest potential for embedding and clustering arrangements.

Chapter 6

Conclusions, Contributions and Future Work

In conclusion, a novel convection method was successfully devised for preparing new platform possibilities, and systemic heating treatment effectively tuned GNP-polymer configurations. In addition, incremental and continuous heat treatments yield different results. Gold-polymer surface nano-composites have been prepared by depositing pre-synthesized gold colloids on the surface of polymer films, by using the thermal convection method. Subsequently, the films hosting the gold aggregates on their surface were heated incrementally at temperatures in the range of 80 to 200^0C and the morphology and spectral properties of the nano-composite were investigated. The results pointed to the following conclusions: the incremental heating, alternating with short cooling periods, leads to the formations of small gold aggregates on the surface, together with a partial or total embedding of a part of the particles into the surface layer of the polymer. This configuration results in a large red shift of the Au LSPR band and, consequently, in an enhanced sensitivity of the nano-composite platform.

The polymers showed the Au LSPR peak response (the shift) increase from 7 nm to 34 nm on average at a temperature range of 175-200°C, and a general absorbance trend of downwards to upwards. The trend may be attributed to an initial aggregation (after deposition) and spreading of gold nanoparticles, and then, as they are increasingly embedded into the polymer surface, absorbance rises. The results are consistent and point towards the general effect of LSPR shifts toward longer wavelengths through aggregation and partial embedding by a gradual heating treatment. This is attributed to changing properties of both particle and polymer. The sinking particles incrementally change depth and degree of polymer envelopment during the course of heating. These changes effect a shift in the absorbance curves. The SEM results show heated samples with particles strongly attached to the polymer and aggregated, and the AFM images and graphs reveal a greater surface roughness for a non-heated sample, indicating a descent of particles into the polymer with heating.

The benefits and novelty of these results and observations, specific to each polymer, are the ability to refine sensing and affinity methods, while selecting the appropriate polymer material for a specific bio-sensing application, by implementing, in accordance with the analyte in question, a treatment of gradual heating in advance. Sensing experiments using different polymer platforms as a substrate for gold nanoparticles are under way and will be the cornerstone of any future extensions of this undertaking. Concerning immediate advantages, the results of this study will be helpful in selecting the most suitable materials for microfluidic sensing. This comprises the essential contribution of this work.

The adsorption of the Green Fluorescent Protein monoclonal antibody on model polymer systems has been investigated. Preliminary results have confirmed that the study of the interaction of GFP with polymers through different methods may be conducive to the evaluation of biocompatibility of polymeric materials for microfluidic applications. More experiments must be undertaken however to confirm the repeatability and precision of these results.

References

[1] D. Erickson, S. Mandal, A. H. J. Yang, and B. Cordovez, "Nanobiosensors: optofluidic, electrical and mechanical approaches to biomolecular detection at the nanoscale," *Microfluidics Nanofluidics*, 2008, 4, pp. 33-52.

[2] C. Monat, P. Domachuk, C. Grillet, M. Collins, B.J. Eggleton, M. Cronin-Golomb, S. Mutzenich, T. Mahmud, G. Rosengarten, and A. Mitchell, "Optofluidics: a novel generation of reconfigurable and adaptive compact architectures," *Microfluid Nanofluid*, 2008, 4, pp. 81-95.

[3] H.Schmidt, and A. R. Hawkins, " The photonic integration of non-solid media using optofluidics," *Nature Photonics*, 2011, 5, pp. 598-604.

[4] J. Zeng, D. Goldfeld, and Y. Xia, "A plasmon assisted optofluidic PAOF) system for measuring photothermal conversion effeciencies of gold nanostructures and controlling an electric switch*," Angewandte Chemie,* 2013, 52, pp. 4169-4173.

[5] D. Psaltis, S. R. Quake, and C. Yang, "Developing optofluidic technology through the fusion of microfluidics and optics," *Nature*, 2006, 442, pp. 381-386.

[6] N. Erdman, L. Schmidt, W. Qin, X. Yang, Y. Lin, M. N. DeSilva, and B. Z. Gao, "Microfluidics-based laser cell-micropatterning system," *Biofabrication*, 2014, 6, pp. 1-9.

[7] S. He, D. Dai, B. Yang, Q. Liu, and Y. Shi, "Small polymer microphotonic integrated devices on silicon substrate," *SPIE*, 2011, pp. 3.

[8] P. B. Laursen, K. Alameh, M. Vasiliev, and N. C. R. Elliott, "Microstructured arrayed microfluidic waveguide structure for infrared radiation focusing and transfer, *Photonics Global*, 2008, 10.1109.

[9] J. Hu, V. Tarasov, A. Agarwal, and L. Kimberling, "Fabrication and testing of planar chalcogenide waveguide integrated microfluidic sensor," *OPTICS EXPRESS*, 2007, 15, pp. 2307 – 2314.

[10] H. Raether , Surface Plasmons on Smooth and Rough Surfaces and on Gratings, *Springer*, Berlin, Germany 1988, 111.

[11] A. S. Urban, M. Fedoruk, M. R. Horton, J. O. Radler, F. D. Stefani, and J. Feldmann, "Controlled nanometric phase transitions of phospholipid membranes by plasmonic heating of single gold nanoparticles," *Nano Letters*, 9, pp. 2903-2908.

[12] http://www.gelifesciences.com/webapp/wcs/stores/servlet/catalog/en/GELifeSciences/brands/biacore/?gclid=Cj0KEQjwyMafBRCU7OCRyc2vitsBEiQAKV4H9BFXB3KbV3Upt_I6lZ3WF7izuxA0Nwanfxu9p9z_FYaAqmN8P8HAQ, accessed: August 2014.

[13] G. M. Whitesides, "The origins and the future of microfluidics," *Nature,* 2006, 442, pp. 368-373.

[14] M. Wang, C. Zhao, X. Miao, Y. Zhao, J. Rufo, Y. J. Loi, T. J. Huang, and Y Xheng, "Plasmofluidics: merging light and fluids at the micro-nanoscale," *Materials Views*, 2015, 35, pp. 4423-4444.

[15] J. R. Moffi tt , Y. R. Chemla , S. B. Smith ,and C. Bustamante, Recent advances in optical tweezers, *Annu. Rev. Biochem*. 2008, 77, pp. 205-228.

[16] G. L. Liu, J. Kim , Y. Lu , and L. P. Lee, Optofluidic control using photothermal nanoparticles, *Nat. Mater.,* 2006, 5, pp. 27-32 .

[17] C. Fang, L. Shao, Y. Zhao, J. Wang, and H. Wu, "A gold nanocrystal/poly (dimethysiloxane) composite for plasmonic heating on microfluidic chips," *Advanced Materials*, 2012, 24, pp. 94-98.

[18] D. A. Boyd , J. R. Adleman , D. G. Goodwin , and D. Psaltis, "Chemical separations by bubble-assisted interphase mass-transfer," *Anal*. *Chem*. 2008, 80, 2452-2456 .

[19] E. B. Ureña , M. P. Kreuzer , S. Itzhakor , H. Rigneault , R. Quidant , D. Oron , and J. Wenger , "Excitation enhancement of a quantum dot coupled to a plasmonic antenna," *Adv*. *Mater*. 2012, 24, 44.

[20] H. Becker, and L. E. Locascio, "Polymer microfluidic devices," *Talanta*, 2002, 56, pp. 267-287.

[21] A. Piruska, I. Nikcevic, S. H. Lee, C. Ahn, W. R. Heinman, P. A. Limbach, and C. J. Seliskar, "The autfluorescence of plastic materials and chips measured under laser irradiation," *Lab Chip*, 2005, 5, pp. 1348-1354.

[22] S. Badilescu, and M. Packirisamy, "Microfluidics-nano-integration for synthesis and sensing," *Polymers*, 2012, 4(2), pp. 1278-1310.

[23] C-W. Tsao, and D. L. DeVoe, "Bonding of thermoplastic polymer microfluidics," *Microfluidics and Nanofluidics*, 2009, 6, pp. 1-16.

[24] P. S. Nunes, and J. P. Kutter, "Cyclic olefin polymers: emerging materials for lab-on-a-chip applications," *Microfluidic Nanofluid*, 2010, 9, pp. 145-161.

[25] A. Toor, "Synthesis and characterization of the gold nanoparticle/SU-8 Nanocomposite Material," thesis at the Univeristy of California at Berkeley, 2015.

[26] C-W Nan, Y Shen, and J. Ma, "Physical properties of composites near percolation," *Annual Review of Materials Research*, 2010, 40, pp. 131–151

[27] S.L.R. Barker, M.J. Tarlov, H. Canavan, J.J. Hickman, and L.E. Locascio, "Control of flow direction in microfluidic devices with polyelectrolyte multilayers," *Analytical Chemistry*, 2000, 72, pp. 4899–4903.

[28] S. Takayama, J.C. McDonald, E. Ostuni, M.N. Liang, P.J.A. Kenis, R.F. Ismagilov, and G.M. Whitesides, "Patterning cells and their environments using multiple laminar fluid flows in capillary networks," *Proceedings of the National Acadamy of Sciences*, 1999, 96, pp. 5545–5548.

[29] R.J. Jackman, D.C. Duffy, E. Ostuni, N.D. Willmore, and G.M. Whitesides, "Fabricating large arrays of microwells with arbitrary dimensions and filling them using discontinuous dewetting," *Analytic Chemistry*, 1998, 70, pp. 2280–2287.

[30] M. D. Borysiak, K. S. Bielawski, N. J. Sniadecki, C.F. Jenkel, B. D. Vogt, and J. D. Posner, "Simple replica micromolding of biocompatible styrenic elastomers," *Lab Chip*, 2003, 13, pp. 2773-3284.

[31] O. G. Abdulah, Y. A. K. Salman, and S. A. Saleem, " In-sity synthesis of PVA/HgS nanocomposite films and tuning optical properties," *Physics and Materials Chemistry*, 2015, 3, pp. 18-24.

[32] http://www.goodfellowusa.com/larger-quantities/polymers/tpx-characteristics/, accessed: June 2016.

[33] N. Abu-Thabit, Y. Umar, E. Ratemi, A. Ahmad, and F. A. Abuilaiwi, " A flexible optical pH sensor based on polysulfone membranes coated with pH-responsibe polyaniline nanofiers," *Sensors*, 2016, 16, pp. 13.

[34] L. Cognet, C.Tardin, D. Boyer, D. Choquet, P.Tamarat, and B. Lounis, "Single metallic nanoparticle imaging for protein detection in cells," *PNAS,* 2003, 100, pp. 11350-11355.

[35] I. Tokareva, S. Minko, J.H. Fendler, and E. Hutte, "Nanosensors based on responsive polymer brushes and gold nanoparticle enhanced transmission surface plasmon resonance spectroscopy," *J. AM. CHEM. SOC.,* 2004, 126, pp.15950-15951.

[36] R.K. Putla,"Monitoring of glass transition at a polymer surface by localized surface plasmon resonance (thesis Oklahoma State University)," 2010, pp. 1-60.

[37] J.H. Teichroeb and J.A. Forrest, "Direct imaging of nanoparticle embedding to probe viscoelasticity of polymer surfaces," *Phys. Rev. Lett.* 2003, 91, 016104.

[38] M. Lahav, A. Vaskevich, and I. Rubinstein, "Biological sensing using transmission surface plasmon resonance spectroscopy," *Am. Chem. Soc.* 2004, *20*, 7365-7367.

[39] E. Hutter and M.P. Pileni, "Hybridization of oligonucleotide-modified silver and gold nanoparticles in aqueous dispersions and on gold films," *J. Phys* 2003, 107, 6497-6499.

[40] U. Kreibig and M.Vollmer, "Optical Properties of Metal Clusters," *Springer*, Berlin, Germany, 1995.

[41] P. Mulvaney, "Surface plasmon spectroscopy of nanosized metal particles," *Langmuir.* 1996, 12, 788-800.

[42] C. Sönnichsen, T. Franzl, T. Wilk, Q. von Plessen, J. Feldmann, O. Wilson, and P. Mulvaney, "Drastic reduction of plasmon damping in gold nanorods," *Phys. Rev. Lett.* 2002, 88, 077402.

[43] Z. Adamczyk, P. Weronski, and E. Musial, "Metal nanoparticles on polymer surfaces: 3. Adsorption kinetics of gold hydrosol particles on polystyrene and poly(2-vinulpyridine)," *J.Colloid Interface Sci.* 2001, 241, pp. 63.

[44] J. Yguerabide and E.E.Yguerabide," Resonance light scattering particles as ultrasensitive labels for detection of analytes in a wide range of applications," *J. Cell. Biochem. Suppl.*2001, 37, 71.

[45] G. Raschke, S. Kowarik, T. Franzl, C. Sonnichsen, T.A. Klar, and J. Feldmann, "Biomelucular recognition based on single gold nanoparticle light scattering," *Nano letter.* 2003, *3,* 935-938.

[46] M.-C. Daniel and D. Astruc, "Gold nanoparticles: assembly, supermolecular chemistry, quantum-size-related properties, and applications toward biology, catalysis, and nanotechnology," *Chem. Rev.* 2004, *104*, 293-346.

[47] D. J. Barber and I. C. Freestrone, "An investigation of the origin of the colour of the lycurgus cup by analytical transmission electron microscopy," *Archaaeometry*, 1990, 32, pp. 33-45.

[48] A. Neri, "L'arte vetraria," Giunti, Firenze 1612.

[49] W. R. Caseri, " In situ synthesis of polymer-embedded nanostructures," Nnaocomposites: In situ Synthesis of Polymer-Embedded Nanostructures, 2014, 1, pp. 45-7.

[50] https://nicoyalife.com/technology/surface-plasmon-resonance/localized-surface-plasmon-resonance-theory/, accessed: July 2016.

[51] L.Nicolais and G. Carotenuto, "Preperation and characterization of metal-polymer nanocomposites," Nanocomposites: In situ Synthesis of Polymer-Embedded Nanostructures, 2014, 1 ,pp. 73-96.

[52] E. Katz and I. Willner, "Integrated nanoparticle-biomolecule hybrid systems: synthesis, properties, and applications," *Angewandte chemie*, 43, pp. 6042 – 6108.

[53] P. K. Jain, K. S. Lee, I. H. El-Sayed, and M. A. El-Sayed, "Calculated absorption and scattering properties of gold nanoparticles of different size, shape, and composition: applications in biological imaging and biomedicine," *J Phys. Chem.*, 2006, 110, pp. 7238-7248.

[54] X. Huang, I. H. El-Sayed, W. Qian, and M. A. El-Sayed, "Cancer cell imaging and photothermal therapy in the near-infrared region by using gold nanorods," *J. Am. Chem. Soc.*, 2006, 128, pp.2115-2120.

[55] N. J. Durr, T. Larson, D. K. Smith, B. A. Korger, K. Sokolov, and A. ben-Yakar, "Two-photon luminescence imaging of cancer cells using molecularly targeted gold nanorods," *Nano letter*, 2007, 7, pp. 941-945.

[56] S. M. Nasir and H. Nur, "Gold nanoparticles embedded on the surface of polyvinyl alcohol layer," *Journal of Fundamental Sciences*, 2008, 4, 245-252.

[57] F-K. Liu, S-Y. H, f-H. Ko, and T-C chu, "Synthesis of golf/poly(methyl methacrylate) hybrid nanocomosites," *Colloids and Surfaces*, 2003, 231, pp. 31-38.

[58] C. Loo, A. Lowery, N. Halas, J. West, and Rebekah Drezek, "Immunotargeted nanoshells for integrated cancer imaging and therapy," *Nano Letters*, 2005, 5, pp. 709-711.

[59] N. Uehara, " Polymer-functionalized gold nanoparticles as versatile sensing materials, *Analytical Sciences*, 2010, 26,pp. 1219-1228.

[60] G. V. Ramesh, S. Porel and T. P. Radhakrishnan, "Polymer thin films embedded with in situ grown metal nanoparticles," *chemical Society Reviews*, 2009, 38, pp. 2646-2656.

[61] Q. Guo, R. Ghadiri, T. Weigel, A. Aumann, E. L. Gurevich, C. Esen, O. Medenbach, W. Cheng, B. Chichkov, and A. Ostendorf, "Comparison of in situ and ex situ methods for synthesis of two-photon polymerization polymer nanocomposites," *Polymers*, 2014, 6(7), pp. 2037-2050.

[62] H. SadAbadi, S. Badilescu, M. Packirisamy, and R. Wüthrich, "Integration of gold nanocparticles in PDMS microfluidics for lab-on-a-chip plasmonic biosensing of growth hormones," *Biosensors and Bioelectronics*, 2013, 10.1016.

[63] M. Alsawafta, S. Badilescu, A. Paneri, V-V Truong and M. Packirisamy, "Gold-poly(methyl methacrylate) nanocomposite films for plasmonic biosensing applications," *Polymers*, 2011, 3, pp.1833-1848.

[64] S. Porel,S. Singh, S. S. Harsha, D. N. Rao, and T.P. Radhakrishnan, "Nanoparticle embedded polymer: in sity synthesis, free-standing films with highly monodisperse silver nanoparticles and optical limiting," *Chem. Mater*, 2005, 17, 9-12.

[65] Okla R. K. Putla, "Monitoring of glass transition at a polymer surface by localized surface Plasmon resonance," Thesis Oklahoma State Univeisty, 2010.

[66] B.W Swatowski, C. M Amb, S. K. Breed, D. J. Deshazer, and W. K Weidner, "Flexible, stable, and easily processable optical silicones for low loss polymer waveguides," Society of Photo-Optical Instrumentation Engineers, 2013, No. 11-3377-01.

[67] I. Cristina, "Polymer Biocompatibility," Intech, 2012, chapter 3, pp. 47-62.

[68] J. Ozhikandathil and M. Packirisamy, "Silica-on-silicon (SOS) waveguide integrated PDMS lab-on-a-chip for quantum dot fluorescence bio-detection," 2012, *Journal of Biomedical Optics*, 17, 017006.

[69] H. Becker and L. Locascio, "Polymer Microfluidic Devices," *Talanta*, 2011, 56, pp. 267-287.

[70] R.J Christie, "Biocompatible Polymers: Design, function and uses," unpublished.

[71] http://www.cytoviva.com/products/hyperspectral-imaging-2/hyperspectral-imaging/, accessed: June 2016.

[72] https://tests.capnhq.gov/ops/archer_training/archer_hsi_tech/Hyperspectral%20&%20High%20Resolution%20Imagery.cfm, accessed: August 2016.

[73] RSoft Design Group, inc. " FullWAVE 6.1 User Guide," 2008.

[74] W. Chew, "Electromagnetic theory on a lattice," *J. Appl. Phys.,* vol. 75, pp. 4843-4850, 1994.

[75] J. Ozhikandathil and M. Packirisamy, "Simulation and implementation of a morphology-tuned gold nano-islands integrated plasmonic sensor," *Sensors.* 2014, *14*, 10497-10513; doi: 10.3390/s140610497

[76] S. Stoenescu, "Optical characterization anisotropic nanostructures by modeling and spectroscopic verification," Thesis at Concordia University, 2013.

[77] T. karakouz, B. M. Maoz, G. Lando, A. Vaskevich, and I. Rubinstein, "Stabilization of gold nanoparticle films on glass by thermal embedding," *Applied Material & Interfaces*, 2011, 3, 978-987.

[78] Darkfield paper V. Pini, P. M. Kosaka, J. J. Ruz, O. Malvar, M. Encinar, J. Tamayo and M. Calleja, "Spatially multiplexed dark-field microscpectrophotometry for nanoplasmonics," *Nature Scientific Reports*, 2016.